

IMPERIAL COLLEGE LONDON

FAULTY OF ENGINEERING

DEPARTMENT OF CIVIL AND ENVIRONMENTAL ENGINEERING

Design of steel trusses by GMNIA with CSM strain limits

Zexu Shao

2021-2022

Abstract

Traditionally, steel truss design typically involves the steps for cross-section classification, estimation of the effective length and individual member capacity check, although these traditional design procedures are optimized for single member design, but the lengthy calculations will normally reduce the design accuracy and efficiency when structure became more complicated.

With the popularization of personal computers, design by second order analysis became a practical design method for structural engineers due to its capacity to capture the second order effects during analysis, but the majority of these second order analysis methods are still rely on the cross-section classification to manipulate the interaction between the bending moment capacity and compressive force resistance, those restrictions for higher classes cross-sections will typically lead to an underestimated ultimate capacity using second order analysis methods.

To overcome these issues and to avoid using computationally demanding shell elements, a newly discovered method, advanced analysis with CSM strain limit is extended to steel Warren truss design in this study. The studied advanced analysis method takes into consideration both geometric and material nonlinearities, which could benefits significantly by capturing the effects of local moment distribution, strain hardening, the element interaction and plasticity spread without additional design checks.

In this study, the literature review of each mentioned analysis method is presented, followed by an evaluation of the accuracy of the studied advanced analysis with CSM strain limits in comparison to the benchmark shell FE model and other alternative advanced analysis methods. Additionally, a worked example illustrating the analysis procedures for each method is attached at Section 5.

Acknowledgements

Since the beginning of my MSc project, I have received a great deal of support and assistance. First and foremost, I would like to express my sincere and deepest gratitude to my supervisor Professor Leroy Gardner, who offered me an opportunity to study and work under his kindly supervision. His incredible excellent guidance, supports and instructive comments were invaluable for this research, I'd say I am blessed to have a professional and knowledgeable supervisor who is always willing to help. Under his supervision, Professor Leroy Gardner aroused my passion which helped me to continue developing on the academic path, and also provided a smooth transition between my MSc life and my next 3 years PhD career.

I also would like to convey my heartfelt gratitude towards to Dr Fiona Walport and Mr Hou Un Chan, whose expertise were very helpful for my research. Without their supports, I would not be able get my hands on the studied advanced analysis quickly. Additionally, they have provided some insightful feedback on this study, and even sent through their unpublished paper, so that I can improve this study.

In addition, I would like to thank Mr John Ward from Robert bird group for his precious comments and instructions on my thesis, those truss examples he has sent through are invaluable for my future research.

Last, but not least, my warm and grateful thanks go to my beloved family for their tremendous supports in every aspect. Without their supports, I might not have the opportunity to be well educated, all my achievements are built on their selfless contributions. The greatest wish in my life is to make my family proud of me.

Contents

1	Introduction	1
2	Literature Review of Analysis Methods	3
2.1	Traditional Method	3
2.2	Studied Advanced Analysis	6
2.2.1	The Continuous Strength Method	6
2.2.2	Influence of High Shear Force	10
2.2.3	The Strain Averaging Approach	11
2.2.4	The Quad-Linear Material Model	12
2.3	Alternative Analysis Method	14
2.3.1	Second order elastic analysis with C-S Check (M4)	14
2.3.2	Second order inelastic analysis with C-S Check (M4)	16
2.4	Comparison of Design Methods	17
3	Finite Element Modelling	19
3.1	Benchmark Shell Finite Element Modelling	19
3.2	Beam Finite Element Modelling	23
4	Results and Discussion	25
4.1	Case Study	26
4.2	Design of Warren Truss	34
5	Worked Example	36
6	Conclusion	44
7	Future Work	45
	Reference	I

List of Figures

1	Buckling curves plotted from Eq (2.3)	4
2	Illustration of the effective length concept (Fieber 2019)	5
3	The base curve of CSM ($\Omega = 15$) (Fieber 2019)	7
4	The quad-linear material model developed by Yun & Gardner (2017)	14
5	Moment capacity-Normal force capacity interaction curve	17
6	Local plate imperfections implemented into I-section (not to scale) (Fieber 2019)	20
7	Adopted residual stress pattern for Benchmark shell FE models(ECCS 1984) .	21
8	The full rigid connection region in shell FE model	22
9	Comparison between the beam and shell finite element model in a simplified truss geometry	24
10	Analysis procedures for different type of analysis mentioned in Section 2 . . .	25
11	Truss geometry, loading and support conditions for Case 1	26
12	Load-deflection paths and predicted ultimate resistances for Case 1	27
13	Comparison of failure point between shell FE mode and beam FE model for Case 1	28
14	Investigation about the CSM strain limit governed cases	29
15	Truss geometry, loading and support conditions for Case 2	30
16	deformed shape for Case 2 truss from shell FE model	30
17	Load-deflection paths and predicted ultimate resistances for Case 2	31
18	Comparison of failure point between shell and beam FE model for Case 3 . . .	32
19	Load-deflection paths and predicted ultimate resistances for Case 3	33
20	Truss geometry, loading and support conditions (Case 4)	34
21	Load-deflection paths and predicted ultimate resistances for Case 4	35
22	Truss geometry, loading and support conditions for worked example	36
23	Internal forces determine from first order global analysis	36
24	The elastic stress distribution at the critical cross-section	38
25	Strain distribution along the diagonal member 6	40
26	GMNIA with nonlinear plastic cross-section check	41
27	GNIA with linear elastic cross-section check	42
28	GNIA with linear plastic cross-section check	43

List of Tables

1	Reference relative bow imperfection β (<i>Eurocode 3 - Design of steel structures 2021</i>)	16
2	Comparison of those advanced analysis mentioned in Chapter 2	18
3	Section sizes for the truss analyzed in Case 1	26
4	Comparisons between the ultimate resistance α_{Shell} of the benchmark shell model, the studied advanced analysis method α_{CSM} and other considered advanced analysis (Case 1)	27
5	Comparisons between the ultimate resistance α_{Shell} of the benchmark shell model, the studied advanced analysis method α_{CSM} and other considered advanced analysis (Case 2)	31
6	Section sizes for the truss analyzed in Case 3	32
7	Comparisons between the ultimate resistance α_{Shell} of the benchmark shell model, the studied advanced analysis method α_{CSM} and other considered advanced analysis (Case 3)	33
8	Section sizes for the truss analyzed in Case 4	34
9	Comparisons between the ultimate resistance α_{Shell} of the benchmark shell model, the studied advanced analysis method α_{CSM} and other considered advanced analysis (Case 4)	35
10	Section sizes for the truss shown in worked example	36

1 Introduction

In terms of steel trusses, it is known as a more economical structural framework comparing to individual steel members, where the applied loads can be resisted primarily by the axial forces of each individual members. Due to its structural functionality, steel trusses are commonly used in long span structures for load-transfer purpose, such as roofs, bridges and transverse buildings (Davison & Owens 2012). Over the last decade, with the increasing complexity of modern truss systems, the conservative traditional method for truss design can no longer satisfy the needs of sustainability, structural designers are thus seeking for an efficient and practical method which the safety and resistance of the truss can be simply assessed, but also economically viable and environmentally friendly.

Traditionally, the load resistance capacity of steel truss is governed by the individual member flexural buckling resistance or cross-section tension resistance, and each individual member should be able to sustain the axial force determined from a first order global analysis that does not considers the load-deformation response of the truss system. Additionally, modern trusses tend to have more complex connection regions, and this will lead to inaccurate results and lengthy calculations using the simplified method, since the estimation of the buckling length L_{cr} is based on the end constraints of each individual member within the truss.

Alternatively, with the help of Finite Elements Analysis, the most representative structural behaviour can be captured by geometrically and materially nonlinear analysis with imperfections (GMNIA), which directly modelling plasticity, residue stress and geometric imperfections using shell elements. However, as the process of modeling truss structure directly using shell elements is cumbersome, so the frame analysis is generally based on modelling the computationally efficient beam finite elements, but the beam finite element is unable to capture the effect of local buckling, which means the lengthy calculations of cross-section classification and cross-section resistance checks are still required. To avoid the complexity of modelling shell elements and the limitation of traditional checks for beam element models, use of strain limits, obtained from the Continuous Strength Method developed by Gardner (2008), has been proposed and been successfully adopted into single member design and portal frame design (Fieber et al. 2019a, Quan et al. 2020, Walport et al. 2021, 2022, Gardner, Yun, Fieber & Macorini 2019).

Unless accounting for the influence of local buckling, the studied advanced analysis with CSM strain limits also take account of the allowable deformation capacity of each individual cross-section and the positive effects from strain hardening, plasticity spreading and the enhanced local stability of the cross-section through strain averaging approach (Fieber et al. 2019b).

In this thesis, an assessment of the studied advanced analysis with CSM strain limits for simple Warren truss structures will be presented, following with the comparison between other available truss analysis methods featured in prEN 1993-1-1, and a systematic worked example of steel truss design by various analysis method will be also provided at the end of this thesis.

2 Literature Review of Analysis Methods

As mentioned in the last chapter, different types of analysis method have been carried out simultaneously in order to compare with the studied advanced analysis method. In prEN 1993-1-1, different types of analysis have been classified to method M0 - M5 according to the extent of the global analysis, imperfections and second order effects (*Eurocode 3 - Design of steel structures* 2021), the method is more comprehensive as the number after letter M is raised, ranging from method (M0) only requires basic cross-sectional resistance check without considering imperfections to method (M5) take into account all in-plane and out-of-plane second order effects, global sway imperfections, torsional effects and local bow imperfections. The following sections will illustrate the analysis methods used in this study separately.

2.1 Traditional Steel Truss Design Approach (M2)

Conventionally, the steel truss design can be divided into two steps; Firstly, the basic force equilibrium analysis is performed to determine the internal forces of individual members (chords and diagonals). Thus, the resistance capacity and stability of each individual member is examined through a series of design checks based on the corresponding cross-section classification, which is governed by the slenderest plate element within the entire cross-section. The purpose of using cross-section classification is to take into account the effects of local buckling on the deformation capacity and resistance of cross-sections. As structural steel sections are slender than the other structural components, and material properties of steel, the majority of steel structures are suspect to compression failure or buckling rather than tension failure. Traditionally, the flexural buckling resistance $N_{b,Rd}$ of compression members are defined by applying a reduction factor χ to the cross-sectional compression resistance shown as:

$$N_{b,Rd} = \frac{\chi A f_y}{\gamma_{M1}} \quad \text{for Class 1, 2 and 3 Cross-sections} \quad (2.1)$$

$$N_{b,Rd} = \frac{\chi A_{eff} f_y}{\gamma_{M1}} \quad \text{for (symmetric) Class 4 Cross-sections} \quad (2.2)$$

In addition, the buckling reduction factor χ is assessed using column buckling curves defined by Eurocode 3 Part 1.1, and it is closely related to the non-dimensional slenderness $\bar{\lambda}$ of the member, the basic formulations for the buckling curves are as given below:

$$\chi = \frac{1}{\Phi + \sqrt{\Phi^2 - \bar{\lambda}^2}} \quad \text{but } \bar{\lambda} \leq 1.0 \quad (2.3)$$

and the corresponding functions for Φ and $\bar{\lambda}$ are shown as below:

$$\Phi = 0.5[1 + \alpha(\bar{\lambda} - 0.2) + \bar{\lambda}^2] \quad (2.4)$$

$$\bar{\lambda} = \sqrt{\frac{Af_y}{N_{cr}}} \quad \text{for Class 1, 2 and 3 Cross-sections} \quad (2.5)$$

$$\bar{\lambda} = \sqrt{\frac{A_{eff}f_y}{N_{cr}}} \quad \text{for Class 4 Cross-sections} \quad (2.6)$$

where A is the cross-sectional area and N_{cr} represents the elastic critical buckling load.

As shown in the formulas above, the buckling reduction factor is also corresponding to the imperfection factor α which is dependent on the type, buckling axis and material properties of the cross-section, the altered shapes of these buckling curves corresponding to different imperfection factors α are shown in the following Fig 1.

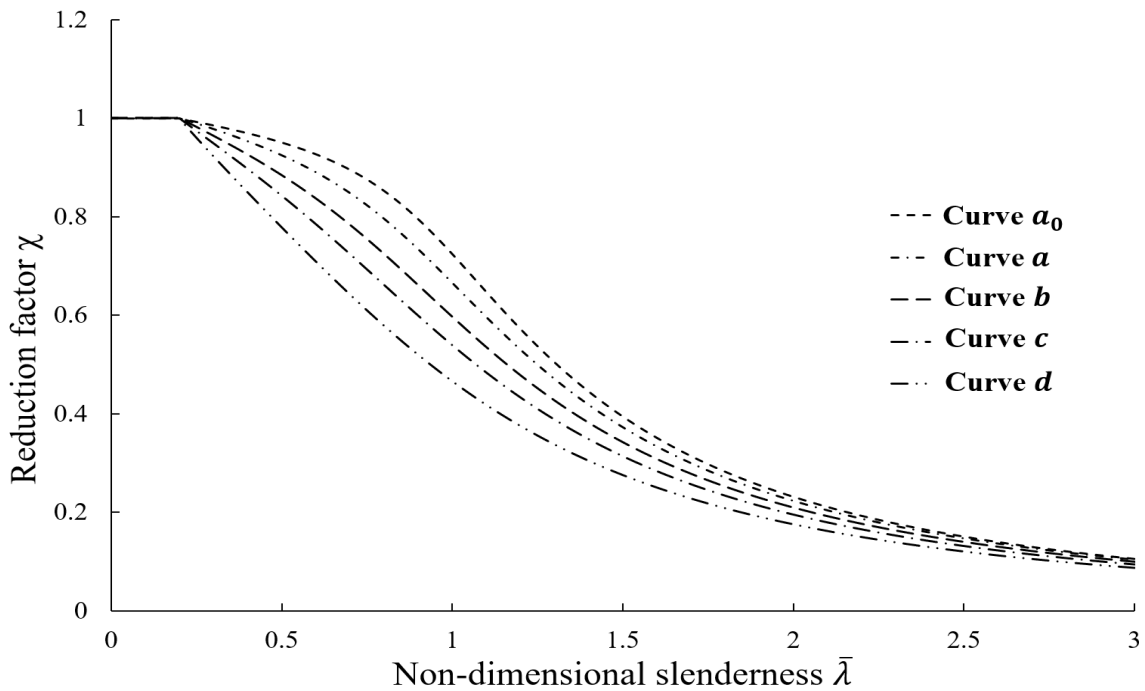


Figure 1: Buckling curves plotted from Eq (2.3)

In addition, the critical buckling load N_{cr} of a compression member can be calculated using the following Eq. (2.7) based on the second moment area I and effective length L_{cr} of the compression member.

$$N_{cr} = \frac{\pi^2 EI}{L_{cr}^2} \quad (2.7)$$

Where determining the value of L_{cr} is one of the main source of uncertainty by using traditional analysis method, the idea of using effective length is to take into account the end constraints and boundary conditions of the compression member. It is clear to see that there are three columns with different length L (original length) in Fig 2, but the effective length L_{cr} for these columns are coincidentally the same due to the different boundary conditions.

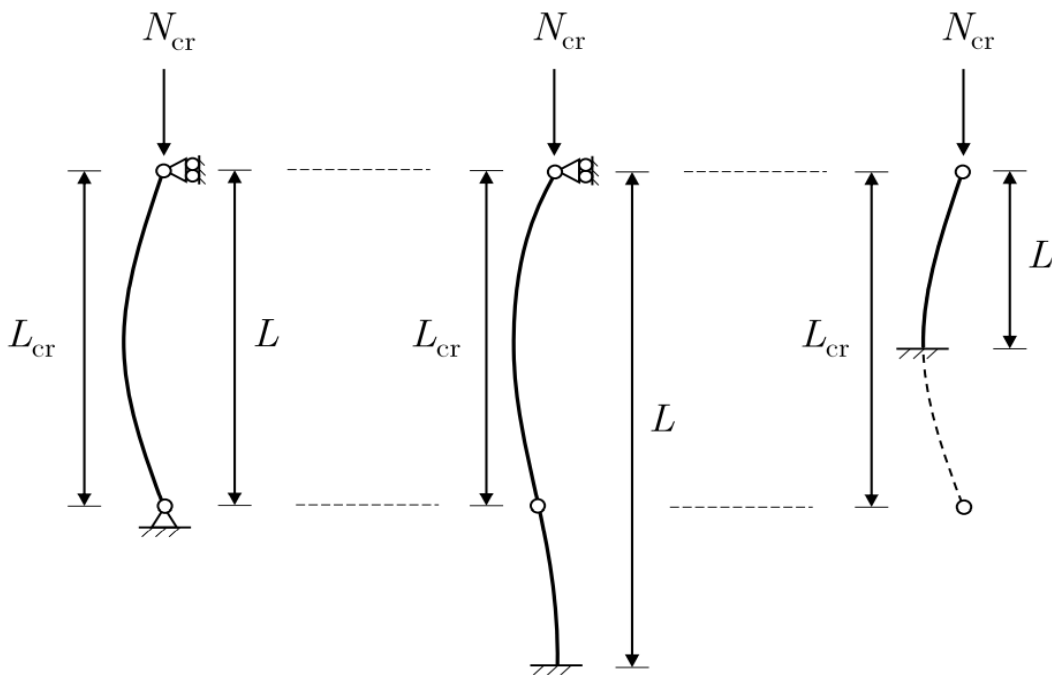


Figure 2: Illustration of the effective length concept (Fieber 2019)

However, in practice steel truss design, the end conditions will be neither ideal pinned or fixed, so overestimate or underestimate the effective length L_{cr} will directly affect the results of buckling resistance, and this phenomenon will be further discussed later by comparing to the results using other analysis methods.

2.2 Advanced Analysis with CSM Strain Limit (M4)

In the upcoming sections, the studied advanced analysis with CSM strain limits is outlined and explained from three aspects; the strain limits defined from the base curve of Continuous Strength Method, the strain averaging approach adopted in the design check and the Quad-Linear material model adopted in the Finite Element model.

2.2.1 The Continuous Strength Method

Continuous Strength Method (CSM) is a deformation-based structural design approach that was developed to overcome the shortcomings of traditional cross-section classifications. The idea behind CSM is to present a continuous relationship between the deformation capacity and the cross-sectional slenderness, and enables the material strain hardening properties to be exploited (Gardner 2008, Fieber 2019). Initially, the CSM was created to account for the advantageous impacts of the high level of non-linearity and strain hardening in stainless steel cross-sections. However, over the years of development, Yun et al. (2018a) also investigated the applicability of continuous strength method on hot-rolled steel cross-sections and discovered that the CSM can also produce more accurate capacity predictions for hot-rolled steel than the conventional analysis method.

For the studied advanced analysis with CSM strain limits, failure is detected at once the maximum longitudinal compressive strain (ε_{Ed}) within the structure has reached the CSM compressive strain limit (ε_{CSM}) that a cross-section can sustain prior to failure, so the relationship between the maximum longitudinal compressive strain ε_{Ed} and CSM compressive strain limit ε_{CSM} should always satisfy Eq. (2.8) at each cross-section within the structure.

$$\frac{\varepsilon_{Ed}}{\varepsilon_{CSM}} \leq 1.0 \quad (2.8)$$

where the CSM compressive strain limit ε_{CSM} is defined by the CSM base curve which is in a relationship between $\varepsilon_{CSM}/\varepsilon_y$ and the local slenderness of the full cross-section $\bar{\lambda}_p$, where ε_y is the yield strain which can be calculated by divide the yield stress f_y by the Young's modulus E (f_y/E). In addition, the CSM base curve has been divided into two parts; for non-slender cross-sections with $\bar{\lambda}_p \leq 0.68$ and for slender cross-section with $\bar{\lambda}_p > 0.68$, the expressions are given as below:

$$\frac{\varepsilon_{csm}}{\varepsilon_y} = \frac{0.25}{\bar{\lambda}_p^{3.6}} \quad \text{but} \leq \left(\Omega, \frac{C_1 \varepsilon_u}{\varepsilon_y} \right) \quad \text{for } \bar{\lambda}_p \leq 0.68 \quad (2.9)$$

$$\frac{\varepsilon_{csm}}{\varepsilon_y} = \left(1 - \frac{0.222}{\bar{\lambda}_p^{1.05}} \right) \frac{1}{\bar{\lambda}_p^{1.05}} \quad \text{for } \bar{\lambda}_p > 0.68 \quad (2.10)$$

For relative stocky cross-sections with $\bar{\lambda}_p \leq 0.68$, a large addition factor could be derived from Eq. (2.9) without setting the upper limits. To avoid the deformation capacity $\varepsilon_{csm}/\varepsilon_y$ exceeding the maximum allowable level of plastic deformation (Ω) and over-prediction of the material strength, two upper limits have been defined in Eq. (2.9), the first limit Ω is a specific design parameter dependent on the designer's preference (tolerance of plastic deformation, purpose of analysis, etc.), the recommended default value of Ω is 15 according to the ductility requirements stated in EN 1993-1-1, and the following Fig. 3 shows the base curve for the entire slenderness range begins at $0 \leq \bar{\lambda}_p \leq 1.4$ using the recommended value of Ω . The second upper limit is related to the constant C_1 for the quad-linear material model explained in Section 2.2.4. Additionally, in the cases of high shear force, relative provisions in EN 1993-1-1 and EN 1993-1-5 are also required to take into account the influence of shear, further details of the relative provisions have been clarified in Quan et al. (2021), section 2.2.2 and an worked example are included in this study to illustrate the shear effect.

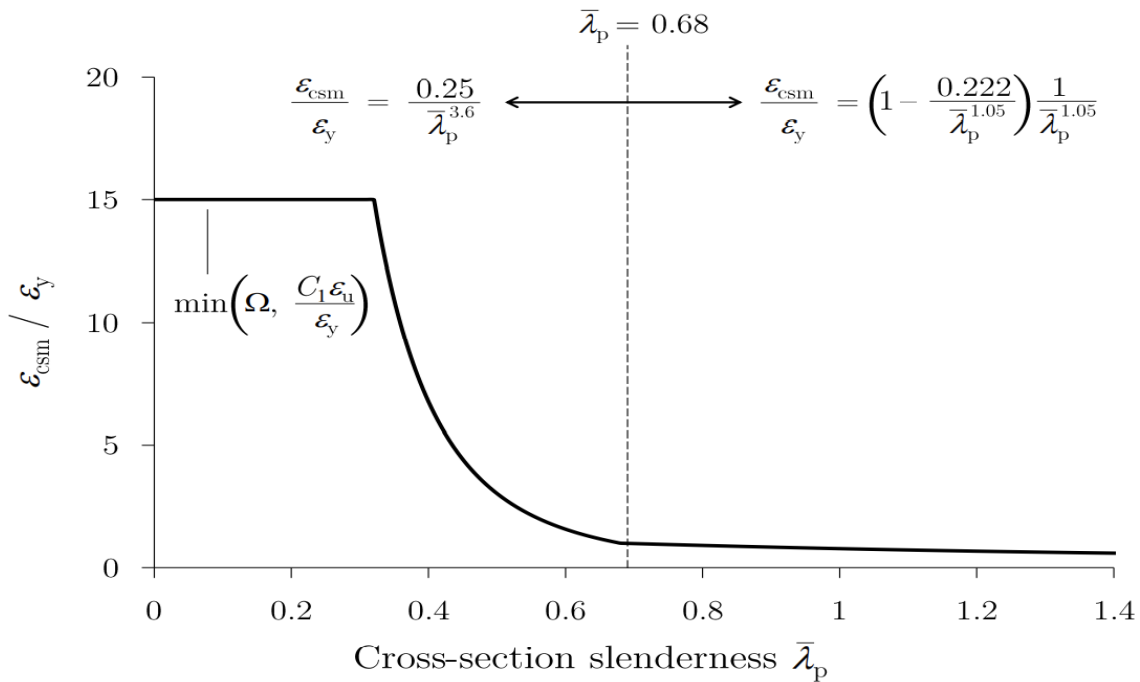


Figure 3: The base curve of CSM ($\Omega = 15$) (Fieber 2019)

In addition, the cross-sectional slenderness $\bar{\lambda}_p$ is used to assess the susceptibility to local instability, and the equation of $\bar{\lambda}_p$ (Eq. 2.11) is dependent on the yield stress f_y and the elastic local buckling stress of the full cross-section $\sigma_{cr,cs}$.

$$\bar{\lambda}_p = \sqrt{\frac{f_y}{\sigma_{cr,cs}}} \quad (2.11)$$

where the elastic critical buckling stress of a cross-section $\sigma_{cr,cs}$ can be easily calculated using the standard plate theory based on the slenderest plate of the cross-section and assuming simply-supported boundary conditions, however, this method will waste part of the cross-sectional capacity which could be utilized through element interaction. As a result, in the rest of the study, the calculation of elastic local buckling stresses of full cross-section will be based on a series of well developed formulae proposed by Gardner, Fieber & Macorini (2019). The general concept used in the calculation of elastic local buckling stress of a full cross-section is to interpolate between the local buckling stresses of the isolated critical plate with fixed and simply supported boundary conditions along the adjoined edges (Gardner, Fieber & Macorini 2019), and the elastic local buckling stress of the full cross-section is shown in Eq. (2.12).

$$\sigma_{cr,cs} = \sigma_{cr,p}^{SS} + \zeta(\sigma_{cr,p}^F - \sigma_{cr,p}^{SS}) \quad \text{where} \quad 0 \leq \zeta \leq 1.0 \quad (2.12)$$

where $\sigma_{cr,p}^{SS}$ is the lower bound in Eq. (2.12), taken as the lowest buckling stress of the isolated plate components with simply-supported boundary conditions along the neighbouring edges (flange $\sigma_{cr,f}^{SS}$ or web $\sigma_{cr,w}^{SS}$), and $\sigma_{cr,p}^F$ is the upper bound in Eq. (2.12) which can be taken similarly from the detached plate components with fixed boundary conditions (flange $\sigma_{cr,f}^F$ or web $\sigma_{cr,w}^F$), the mathematical expressions of the elastic buckling stress for the detached plate with simply-supported and fixed support conditions can be found below.

$$\sigma_{cr,p}^{SS} = \min(\beta_f \sigma_{cr,f}^{SS}, \beta_w \sigma_{cr,w}^{SS}) \quad (2.13)$$

$$\sigma_{cr,p}^F = \min(\beta_f \sigma_{cr,f}^F, \beta_w \sigma_{cr,w}^F) \quad (2.14)$$

where β_f and β_w are the load correction factors related to the ratio of maximum design compressive stress in the cross-section and the maximum compressive stress in flange or web, given as below.

$$\beta_f = \frac{\sigma_{\max,cs}}{\sigma_{\max,f}} \quad \beta_w = \frac{\sigma_{\max,cs}}{\sigma_{\max,w}} \quad (2.15)$$

In addition, the buckling stress for an isolated plate can be derived from the general expression Eq. (2.16).

$$\sigma_{cr,p} = k \frac{\pi^2 E}{12(1-\nu^2)} \left(\frac{t}{b} \right)^2 \quad (2.16)$$

where k represents the buckling coefficient of internal and outstand plates with simply-supported or fixed boundary conditions along the adjacent edges, and the formula of the coefficient of buckling k have been tabulated in EN 1993-1-5 and been extended by Gardner, Fieber & Macorini (2019). Furthermore, as this study focuses mainly on the structural behaviour of I-section trusses subjected to principal axis bending and compression, only the expressions for the interaction coefficients that have been used in this study are presented below.

$$\zeta = 0.15 \frac{t_f}{t_w} \phi \geq \frac{t_w}{t_f} (0.4 - 0.25\phi) \quad \text{Flange critical } (\phi < 1) \quad (2.17)$$

$$\zeta = \frac{t_f}{t_w} \left(0.45 - \frac{0.3}{\phi^2} \right) \quad \text{Web critical } (\phi \geq 1) \quad (2.18)$$

where the symbol ϕ in Eq. (2.17 & 2.18) is a governing term which quantifies the susceptibility of the web and the flange plates to local buckling, and the expressions for ϕ are given as below:

$$\phi = \frac{\beta_f \sigma_{cr,f}^{SS}}{\beta_w \sigma_{cr,w}^{SS}} = \left(\frac{\sigma_{cr,f}^{SS}}{\sigma_{cr,w}^{SS}} \right) \left(\frac{\sigma_{\max,w}}{\sigma_{\max,f}} \right) \quad (2.19)$$

$$\phi = \frac{\sigma_{cr,f}^{SS}}{\sigma_{cr,w}^{SS}} \quad \text{if } \sigma_{\max,f} = \sigma_{\max,w} \quad (2.20)$$

2.2.2 Influence of High Shear Force

According to the conventional design check stated in EN 1993-1-1, the shear capacity check of a cross-section must satisfy the following expression:

$$\frac{V_{Ed}}{V_{pl,Rd}} \leq 1.0 \quad (2.21)$$

where V_{Ed} is the design shear force, and the $V_{pl,Rd}$ is the plastic shear resistance of the cross-section. Additionally, EN 1993-1-1 suggested that a reduction factor should be applied to the bending capacity once the design shear force V_{Ed} exceeds half of the plastic shear capacity $V_{pl,Rd}$, and the bending moment is thus determined based on the decreased yield stress $(1 - \rho)f_y$ to account the shear area within the cross-section, the reduction factor ρ can be expressed as below.

$$\rho = \left(\frac{2V_{Ed}}{V_{pl,Rd}} - 1 \right)^2 \quad (2.22)$$

Similar approach has adopted in the studied CSM strain limit method, a reduction factor ρ_{csm} is thus required to take into consideration the effects of high shear force. For the case of a cross-section experiencing high shear, the relationship between the maximum longitudinal compressive strain ε_{Ed} and CSM compressive strain limit ε_{csm} should now satisfy Eq. (2.23) given below (Quan et al. 2021).

$$\frac{\varepsilon_{Ed,Lb}}{\rho_{csm}\varepsilon_{csm}} \leq 1.0 \quad \text{for} \quad V_{Ed} > 0.5V_{pl,Rd} \quad (2.23)$$

As the calculation of the CSM reduction factor ρ_{csm} is modified based on the reduction factor ρ provided in EN 1993-1-1, and the CSM reduction factor is directly applied on the compressive strain limit, so a separate design check is still required to satisfy Eq. (2.22). For a cross-section experiencing the shear force not greater than 50 percent of the plastic shear resistance $V_{pl,Rd}$, the CSM reduction factor shall be simply taken as 1. The expressions for the 2 cases are given as below in Eq. (2.24).

$$\rho_{csm} = \begin{cases} 1 & \text{for } V_{Ed} \leq 0.5V_{pl,Rd} \\ \frac{0.5}{0.5+\rho} & \text{for } V_{Ed} > 0.5V_{pl,Rd} \end{cases} \quad (2.24)$$

2.2.3 The Strain Averaging Approach

The resultant CSM strain limits could be directly compared to the strain outputs derived by finite element analysis under normal conditions. In certain instances, however, the existence of a local moment gradient over the member length may improve the local stability of the cross-section (Fieber 2019). In order to take into account the advantageous effects of local moment gradients, the CSM strain limit is applied to the averaged strain generated from FE analysis over the characteristic length of the member $L_{b,cs}$, where the expressions of the strain averaging approach are given as below.

$$\frac{\varepsilon_{Ed,Lb}}{\varepsilon_{csm}} \leq 1.0$$

$$\varepsilon_{Ed,Lb} = \frac{1}{n} \sum_{i=1}^n \varepsilon_i \quad \text{and} \quad n \geq 1 \quad (2.25)$$

where $\varepsilon_{Ed,Lb}$ is the mean design compressive strain of n completed elements lying inside the corresponding local buckling half-wavelength $L_{b,cs}$, and additional step of considering weighted average strain should be carried out for the case of unequal element length.

In addition, the elastic local buckling half-wavelength $L_{b,cs}$ could be determined numerically using finite strip analysis (Li & Schafer 2010) or using the analytical expressions proposed by Fieber et al. (2019b) which is developed in a series with the elastic local buckling stress of the full cross-section (Gardner, Fieber & Macorini 2019). The general approach of the elastic local buckling half-wavelength is similar to the one adopted in the calculation of the elastic local buckling stress, both expressions are tend to interpolate between a lower and upper limits, the general form of $L_{b,cs}$ can be expressed as:

$$L_{b,cs} = L_{b,p}^{SS} - \zeta (L_{b,p}^{SS} - L_{b,p}^F) \quad \text{where} \quad 0 \leq \zeta \leq 1 \quad (2.26)$$

where the interaction coefficient is again expressed by the symbol ζ , $L_{b,p}^{SS}$ and $L_{b,p}^F$ are the half-wavelength envelopes of the isolated critical plates with simply-supported and fixed boundary conditions, the following Eq. (2.27) can be used to determine the buckling half-wavelengths of the isolated plates with fixed boundary or simply-supported conditions along their neighbouring edges.

$$L_{b,p} = k_{Lb} b_p \quad (2.27)$$

where k_{Lb} is the coefficient depends on the boundary conditions and the applied stress distribution of the isolated plate, and the expressions of k_{Lb} for internal and outstand plates with simply-supported and fixed edge conditions are tabulated in the paper published by Fieber et al. (2019b). However, comparing to the elastic buckling stress calculations, an additional transition function η need to be adopted on the basis of calculated half-wave length in order to overcome the discontinuity of the local buckling half-wavelength at $\phi = 1$, the general expressions are given as below.

$$L_{b,p}^{SS} = L_{b,w}^{SS}\eta + L_{b,f}^{SS}(1 - \eta) \quad (2.28)$$

$$L_{b,p}^F = L_{b,w}^F\eta + L_{b,f}^F(1 - \eta) \quad (2.29)$$

Furthermore, the interaction coefficient ζ used in Eq. (5.1) is the same one illustrated in Section 2.2.1 for calculation of elastic local buckling stress of the full cross-section, and can be taken directly from Eq. (2.17 & 2.18).

2.2.4 The Quad-Linear Material Model

As the increasing use of advanced computational techniques in structural analysis, and the ability of computational software to capture the stress and strain changes more accurately, in order to maximise the benefits of advanced analysis, a more accurate material model is required to represent the stress-strain response of hot-rolled structural steels during analysis. Therefore, in this study, a quad-linear material model for hot-rolled structural steel developed by Yun & Gardner (2017) will be employed to define the strain-hardening behaviour and yield plateau length. Unlike the other stress-strain models, the quad-linear material model developed by Yun & Gardner (2017) has been successfully adopted into the proposed advanced analysis for hot-rolled carbon steel cross-sections subjected to bending, compression and combined loading (Yun et al. 2018a,b, Fieber et al. 2019a, Gardner, Yun, Fieber & Macorini 2019), its simplicity and precise stress-strain relationship makes it ideal for those FE models that consider material nonlinearities. Equation 2.30 can be used to define the stress-strain expressions of the quad-linear material model.

$$\varepsilon = \begin{cases} E\varepsilon & \text{for } \varepsilon \leq \varepsilon_y \\ f_y & \text{for } \varepsilon_y < \varepsilon \leq \varepsilon_{sh} \\ f_y + E_{sh}(\varepsilon - \varepsilon_{sh}) & \text{for } \varepsilon_{sh} < \varepsilon \leq C_1\varepsilon_u \\ f_{C_1\varepsilon_u} + \frac{f_u - f_{C_1\varepsilon_u}}{\varepsilon_u - C_1\varepsilon_u}(\varepsilon - C_1\varepsilon_u) & \text{for } C_1\varepsilon_u < \varepsilon \leq \varepsilon_u \end{cases} \quad (2.30)$$

From Eq. (2.30), it is evident that the entire stress-strain curve can be defined by just three regularly used parameters: the yield stress f_y , the Young's modulus E and the ultimate stress f_u . Based on the three commonly used parameters, the followings can be easily derived using Eq. (2.31–2.33); ε_{sh} is the strain when the behaviour of strain hardening first occurs, ε_u is the ultimate strain, E_{sh} is the strain hardening modulus, $f_{C_1\varepsilon_u}$ is the corresponding stress of strain $C_1\varepsilon_u$ which is located at the intersection point of the third stage of the quad-linear model as shown below in Fig. 4.

$$\varepsilon_{sh} = 0.1 \frac{f_y}{f_u} - 0.055 \quad \text{but} \quad 0.015 \leq \varepsilon_{sh} \leq 0.03 \quad (2.31)$$

$$\varepsilon_u = 0.6 \left(1 - \frac{f_y}{f_u} \right) \quad \text{but} \quad \varepsilon_u \geq 0.06 \quad (2.32)$$

$$E_{sh} = \frac{f_u - f_y}{C_2\varepsilon_u - \varepsilon_{sh}} \quad (2.33)$$

Additionally, C_1 and C_2 are experimentally calibrated constant which is related to the ultimate strain ε_u and ε_{sh} , the expressions for C_1 and C_2 are given in Eq. (2.34 & 2.35)

$$C_1 = \frac{\varepsilon_{sh} + 0.25(\varepsilon_u - \varepsilon_{sh})}{\varepsilon_u} \quad (2.34)$$

$$C_2 = \frac{\varepsilon_{sh} + 0.4(\varepsilon_u - \varepsilon_{sh})}{\varepsilon_u} \quad (2.35)$$

Based on the parameters required for the quad-linear model, a representative quad-linear material model can be plotted to demonstrate the behaviour of strain hardening and yield plateau, as demonstrated in Fig. 4.

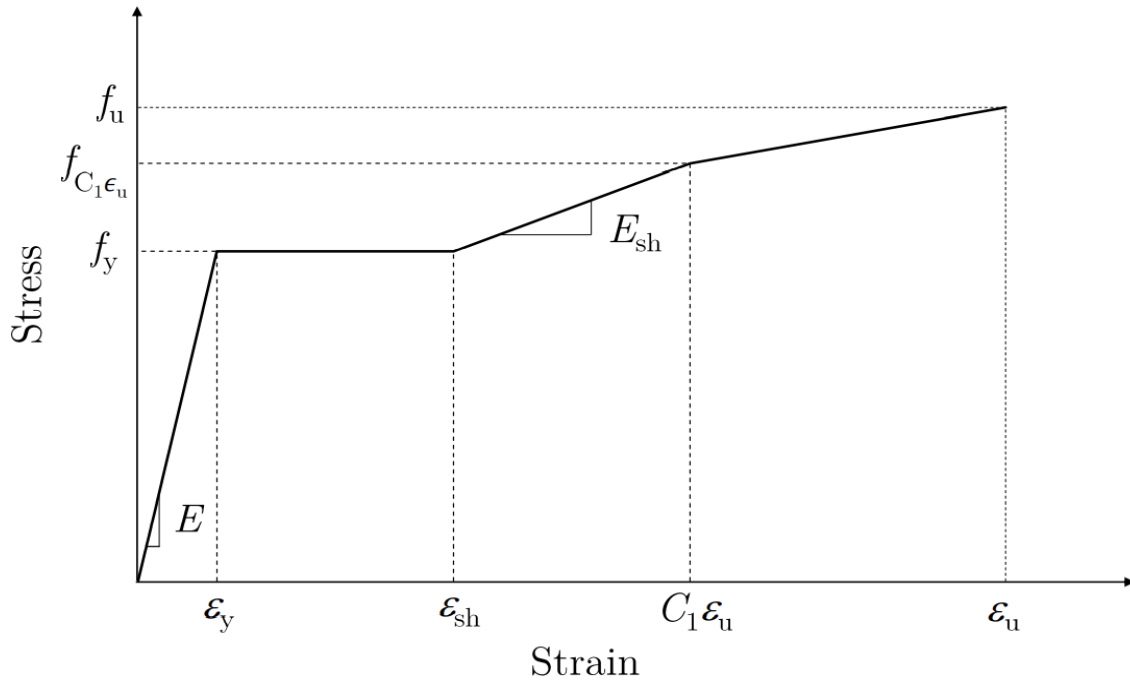


Figure 4: The quad-linear material model developed by Yun & Gardner (2017)

2.3 Other Available Analysis methods in prEN 1993-1-1

Any method that is able to capturing the stability and strength of a structural system and each of its individual members, without the need for additional member capacity checks, can be described as advanced analysis (Chen 2008). Among the literature, there are some other analysis methods could be also classified as 'advanced' which have been used extensively; ranging from the simplest Elastic-Plastic hinge method (Liew 1992) to the most refined Plastic-zone method (Ziemian et al. 1992). In order to compare the proposed advanced analysis methods, some common analysis methods accepted in the prEN 1993-1-1 will be illustrated in the following sections simultaneously.

2.3.1 Second order elastic analysis with C-S Check (M4)

Second order elastic analysis is also known as geometrically nonlinear analysis with imperfections (GNIA), which can take into account the second order effects resulted due to sway imperfections and bow imperfections. This type of analysis was widely used in the early twenty-first century (Chan & Chen 2005, Chan & Cho 2008, Cho & Chan 2008) as it could significantly improve the efficiency of design compared to traditional analysis methods. However, the lack of material non-linearity within the computational model still cannot taking the

advantages from the process of strain hardening.

During the analysis, Chan & Chen (2005) suggested that every element along the member length is required to satisfy the section capacity check shown in Eq. (2.36).

$$\frac{P}{f_y A} + \frac{(M_y + P\Delta_y + P\delta_y)}{M_Y} + \frac{(M_z + P\Delta_z + P\delta_z)}{M_Z} = \varphi \leq 1 \quad (2.36)$$

where f_y is the yield strength, P is the applied load, A is the area of the cross-section, M_y and M_z are the design moments about the principle axis y or z respectively, $P(\delta_z + \Delta_z)$ and $P(\delta_y + \Delta_y)$ are the second order effects about the y and z axis caused by the change of member geometry (imperfections). Additionally, M_Y and M_Z are the elastic/plastic cross-sectional bending moment resistance which is related to the cross-sectional properties. Normally, as the FE package can automatically account the second order effects, and the output can be directly taken as the design axial force or bending moment, so a simplified version of Eq. (2.36) is given in prEN 1993-1-1 shown as below:

$$\frac{N_{Ed}}{N_{Rd}} + \frac{M_{y,Ed}}{M_{y,Rd}} + \frac{M_{z,Ed}}{M_{z,Rd}} \leq 1, 0 \quad (2.37)$$

where in the above Eq. (2.37), N_{Rd} represents the cross-section compressive resistance. For a linear plastic cross-section check with Class 1 or 2 cross-sections, then $M_{y,Rd}$ and $M_{z,Rd}$ are the plastic moment capacity. Similarly, $M_{y,Rd}$ and $M_{z,Rd}$ should be taken as the elastic moment capacity if linear elastic cross-section check is required.

Furthermore, as this study is restricted at investigating single plane truss system, out of plane failure mechanisms are out of the concern, so the bow imperfection used in second order elastic analysis is taken as the tabulated equivalent bow imperfection in prEN 1993-1-1 to account for the residual stresses and initial geometric nonlinearity, the general expressions are given as below:

$$e_0 = \frac{\alpha}{\varepsilon} \beta L \quad (2.38)$$

where L is the length of the member, α is the imperfection factor related to the relevant buckling curve according to Table 8.2 in prEN 1993-1-1, ε is the material parameter equals to $\sqrt{235/f_y}$ and β is the reference relative bow imperfection can be taken from Table 1.

Table 1: Reference relative bow imperfection β (*Eurocode 3 - Design of steel structures 2021*)

Buckling about axis	Elastic cross-section verification	Plastic cross-section verification
y-y	1/110	1/75
z-z	1/200	1/68

2.3.2 Second order inelastic analysis with C-S Check (M4)

Second order inelastic analysis, also referred to as Geometrically and Materially nonlinear analysis with imperfections, will result in more precise predictions of the complete load-deformation response of a structural system. As beam finite elements models is adopted again for this type of analysis, so additional C-S check is still required in this case. However, unlike the C-S check used in GNIA analysis, additional capacity could be achieved by carrying out nonlinear cross-section check for Class 1 and Class 2 cross sections, and the bending moment resistance M_{Rd} can be calculated using the formula given as below:

$$M_{N,y,Rd} = M_{pl,y,Rd} \frac{1-n}{1-0,5a} \quad \text{but} \quad M_{N,y,Rd} \leq M_{pl,y,Rd} \quad (2.39)$$

$$M_{N,z,Rd} = M_{pl,z,Rd} \quad \text{for} \quad n \leq a \quad (2.40)$$

$$M_{N,z,Rd} = M_{pl,z,Rd} \left[1 - \left(\frac{n-a}{1-a} \right)^2 \right] \quad \text{for} \quad n > a \quad (2.41)$$

where

$$n = N_{Ed}/N_{pl,Rd} \quad (2.42)$$

$$a = (A - 2bt_f)/A \quad \text{but} \quad a \leq 0,5 \quad (2.43)$$

where A is the surface area of the cross-section, t_f is the flange thickness and b is the width.

In order to visualize the capacity increment by using Nonlinear C-S check, the moment capacity and the normal force capacity ($M - N$) has been plotted in a same graph with linear $M - N$ interaction curve for a cross-section with $a = 0.5$ shown in Fig 5.

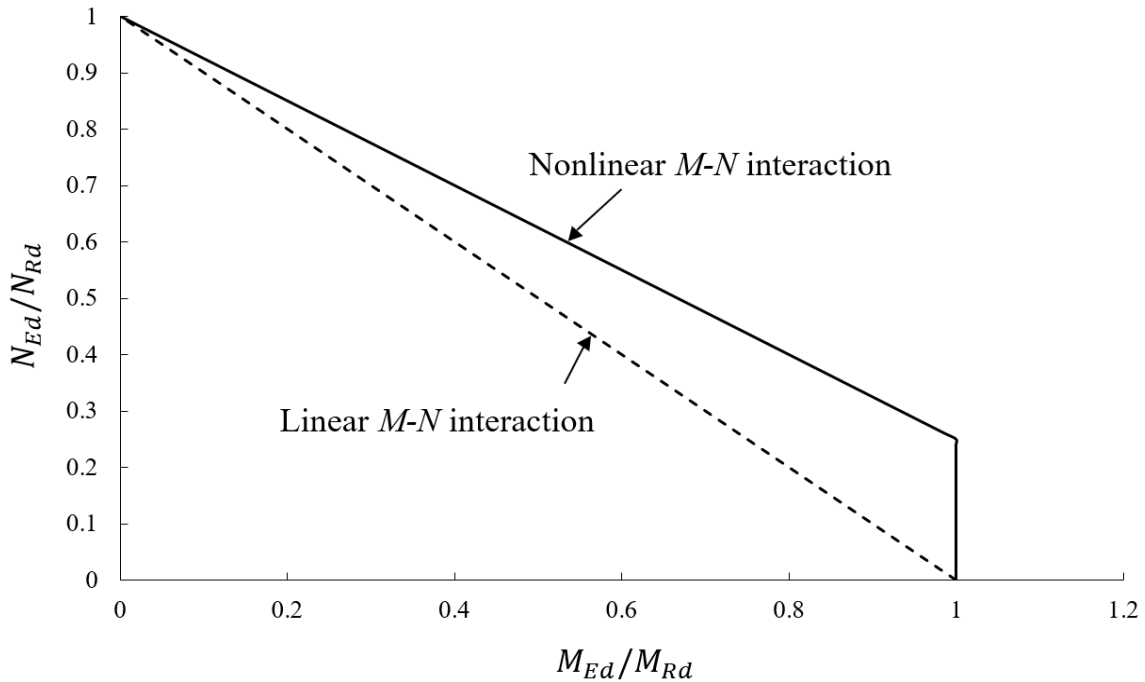


Figure 5: Moment capacity-Normal force capacity interaction curve

Additionally, the equivalent bow imperfection listed in Table 1 were developed on the basis of second order elastic analysis, inappropriate use of equivalent bow imperfections into second order inelastic analysis may lead to an over-predicted or under-predicted results. The GMNIA with nonlinear C-S check would therefore employ a recently defined equivalent bow imperfections especially designed for second-order inelastic analysis (Walport et al. 2020), the general expressions of the equivalent bow imperfections developed by Walport et al. (2020) are given as below:

$$\frac{e_0}{L} = \alpha\beta \quad \text{but} \quad \frac{e_0}{L} \geq \frac{1}{1000} \quad (2.44)$$

Where β is generally recommended as 1/150 for carbon steel, and the imperfections can be directly modelled as a half-sine wave or scaled to suitable elastic buckling modes.

2.4 Comparison of Design Methods

For those advanced analysis methods mentioned in this chapter, an comparison has been carried out for the differences between the key parameters of those advanced analysis methods, also include the benchmark shell finite element model mentioned before, an overview of the comparison is shown in the following Table2.

Table 2: Comparison of those advanced analysis mentioned in Chapter 2

	Design method			
	Elastic design		Plastic design	
Global analysis	LA	GNIA	GNIA	GMNIA*
Method	M2	M4	M4	M4
Local Imperfection	-	-	-	-
Bow Imperfection	-	$e_{0,el,tab}$	$e_{0,pl,tab}$	$L/1000$ $e_{inelastic}$
Residual stress	-	-	-	ECCS residual stress pattern
Material model	Perfect elastic model		Quad-linear stress strain curve	
Element type	Beam finite element (B31 OS)		Shell finite element	B31 OS
Cross-section resistance	EC3 Member Checks	Linear Elastic C-S Check	Linear Plastic C-S Check	Nonlinear/Linear Plastic C-S Check
			Peak Load	CSM Strain Limit

* Studied advanced analysis with CSM strain limits.

** Plate imperfections stated in EN 1993-1-5

3 Finite Element Modelling

As mentioned in last chapter, the advanced analysis methods require the assistance of computational power, so Abaqus as a general FE package is used in this work to evaluate the precision of the studied advanced analysis with CSM strain limit. Firstly, the approaches adopted in modelling the benchmark shell FE models will be illustrated in Section 3.1, followed by the beam FE models which is specifically designed for the proposed CSM strain limit method, and the simplified versions of the beam FE model will be implemented to the other advanced analysis methods with C-S check.

3.1 Benchmark Shell Finite Element Modelling

The concept of directly modelling structural systems with shell elements was inspired by Gardner, Yun, Fieber & Macorini (2019), Fieber et al. (2019a) and Walport et al. (2022), where the accuracy of using shell FE models to capture the full load-deformation behaviour has been successfully validated against experimental results for the cases of individual structural member and portal frame analysis. Therefore, shell FE models will be adopted again in this study as the benchmark results for truss analysis.

For the shell FE model, the reduced integration of the general four-noded shell elements S4R expressed in Abaqus is adopted in this study, and each web and flange is assigned 12 such shell elements, the web and flange are then connected together using the Abaqus defined connector (*MPC BEAM) to form the desired I-section, thus, the member has been meshed along the axis by ensuring the aspect ratio of element was close to 1. In addition, the plate thickness t_w and t_f were assigned respectively for the web and flange plates for I-sections.

Furthermore, since the benchmark shell FE model is supposed to simulate the real structural behaviour as close as possible, it is assumed that the member initial out-of-straightness is $l/1000$ (Walport et al. 2022) rather than the equivalent bow imperfections mentioned before, and the local plate imperfection is modelled in a sinusoidal shape for both web δ_{web} and flange δ_{flange} shown in Fig 6. The amplitude of local plate imperfections are assumed to be equal to $c/200$ for both web and flange according to the plate imperfection stated in Annex C of EN 1993-1-5, where c is the width or height of the flange or web plate, and the number of sinusoidal waves along each member was calculated as the nearest integer of local buckling half-wavelength $L_{b,cs}$ that could fit inside the member length. (Fieber et al. 2019a).

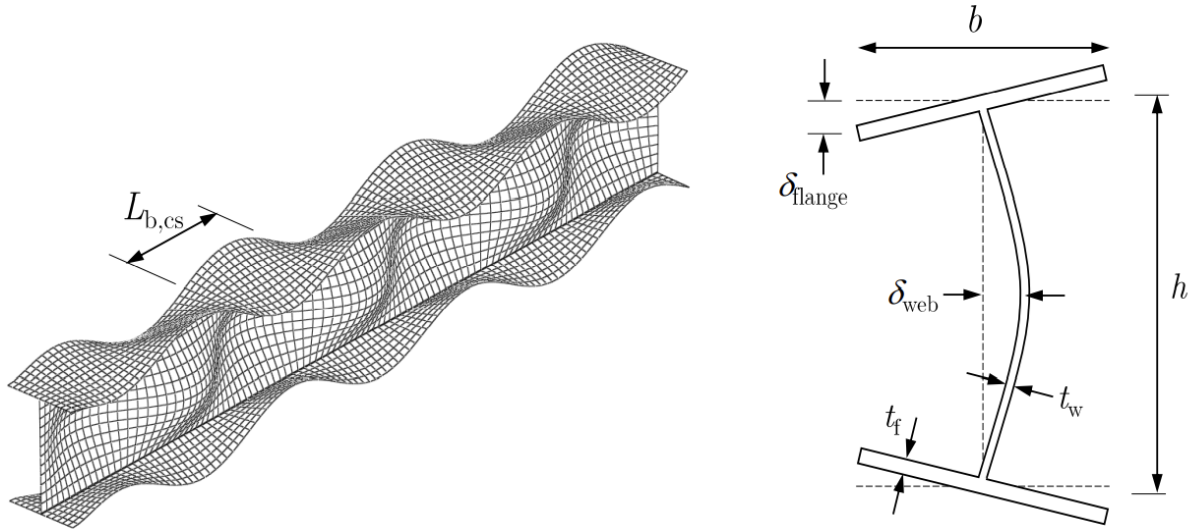


Figure 6: Local plate imperfections implemented into I-section (not to scale) (Fieber 2019)

The quad-linear material model discussed previously is incorporated into the shell FE models by means of a multi-linear approximation characterised by 135 intervals, and the engineering stress strain curves were transformed to truss stress and strains using Eq. (3.1) and Eq. (3.2) respectively as required by Abaqus.

$$\varepsilon_{\text{true}} = \ln(1 + \varepsilon_{\text{eng}}) \quad (3.1)$$

$$\sigma_{\text{true}} = \sigma_{\text{eng}} (1 + \varepsilon_{\text{eng}}) \quad (3.2)$$

Additionally, the nonlinear material response is also required to be converted to true plastic strains $\varepsilon_{\text{true}}^{\text{pl}}$ using the expression given by Eq. (3.3)

$$\varepsilon_{\text{true}}^{\text{pl}} = \varepsilon_{\text{true}} - \frac{\sigma_{\text{true}}}{E} \quad (3.3)$$

As the initial geometric imperfections is taken as a relative conservative value which can not take into account the effects due to other alternative sources, residual stress is still required to be directly modelled in the shell FE models. ECCS residual stress pattern was assumed, and were explicitly modelled as an initial stress condition in Abaqus. During modelling, an additional analysis step was created prior to the loading step to allow the residual stresses to self-equilibrate, the adopted ECCS residual stress model can be found below in Fig 7, and the amplitude of the residual stress σ_{rs} is related to the aspect ratio h/b of the cross-section.

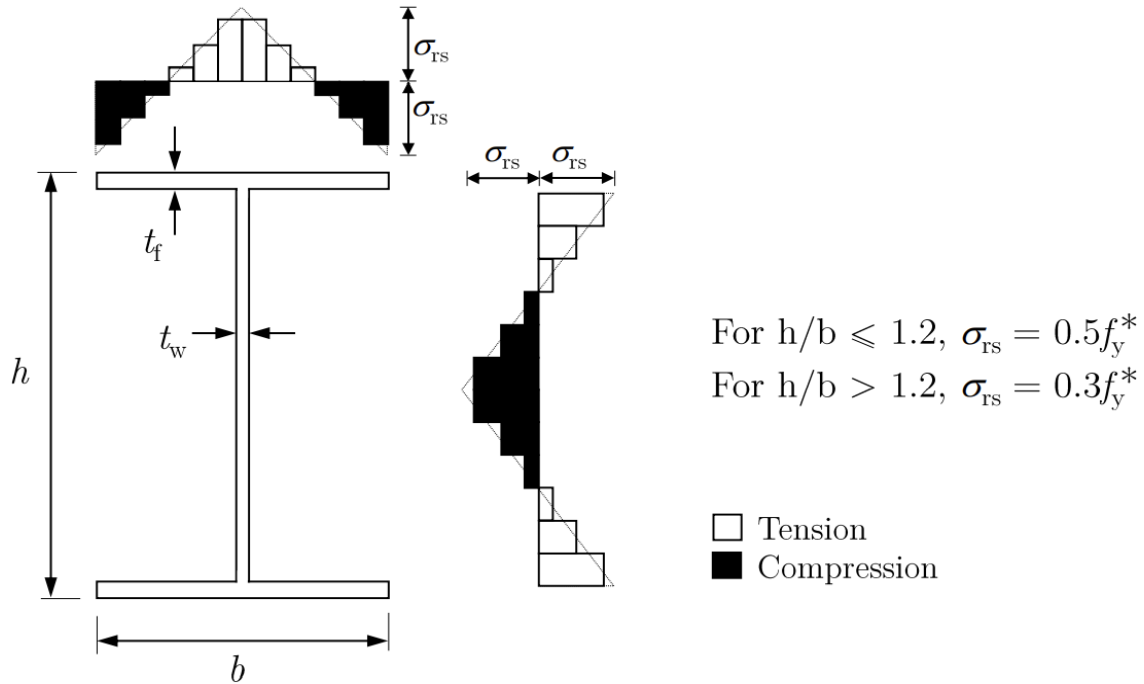


Figure 7: Adopted residual stress pattern for Benchmark shell FE models(ECCS 1984)

Additionally, the formed I-sections were aligned at assigned geometry, and the end nodes at the centroid of each member were defined as **Slave* and **Master* nodes in Abaqus for connection purpose. Normally, the end nodes in chord member will be defined as **Master* node in the order of left to right, the rest of the members will then be connected to that **Master* node simultaneously, and all nodes of the member at end cross-section were coupled to the **Master* node, so different support conditions can be achieved by manipulate about the number of degrees of freedom at the assigned **Master* node.

Currently, the beam FE model connects the diagonal member to the chord member using **MPC BEAM* in Abaqus which avoided the phenomenon of overlapping between diagonal members and chords, but also makes the connection region became unrealistically full rigid as the Abaqus defined **MPC BEAM* is a rigid connector. To represents this rigid connection region into the benchmark shell FE model, the top flange and the bottom flange are connected using **MPC TIE* in the connection region, and the size of connection region is defined from the bottom flange of the left diagonal to the top flange of the right diagonal as shown in the following Fig 8. An additional vertical stiffener is modelled at the position of applied point load, the thickness of the vertical stiffener is identical to the web thickness, and attached to the I-section web using **MPC TIE* connector. Finally, the GMNIA analysis (shell FE model) of the truss system can then be solved by using the modified Riks arc length algorithm.

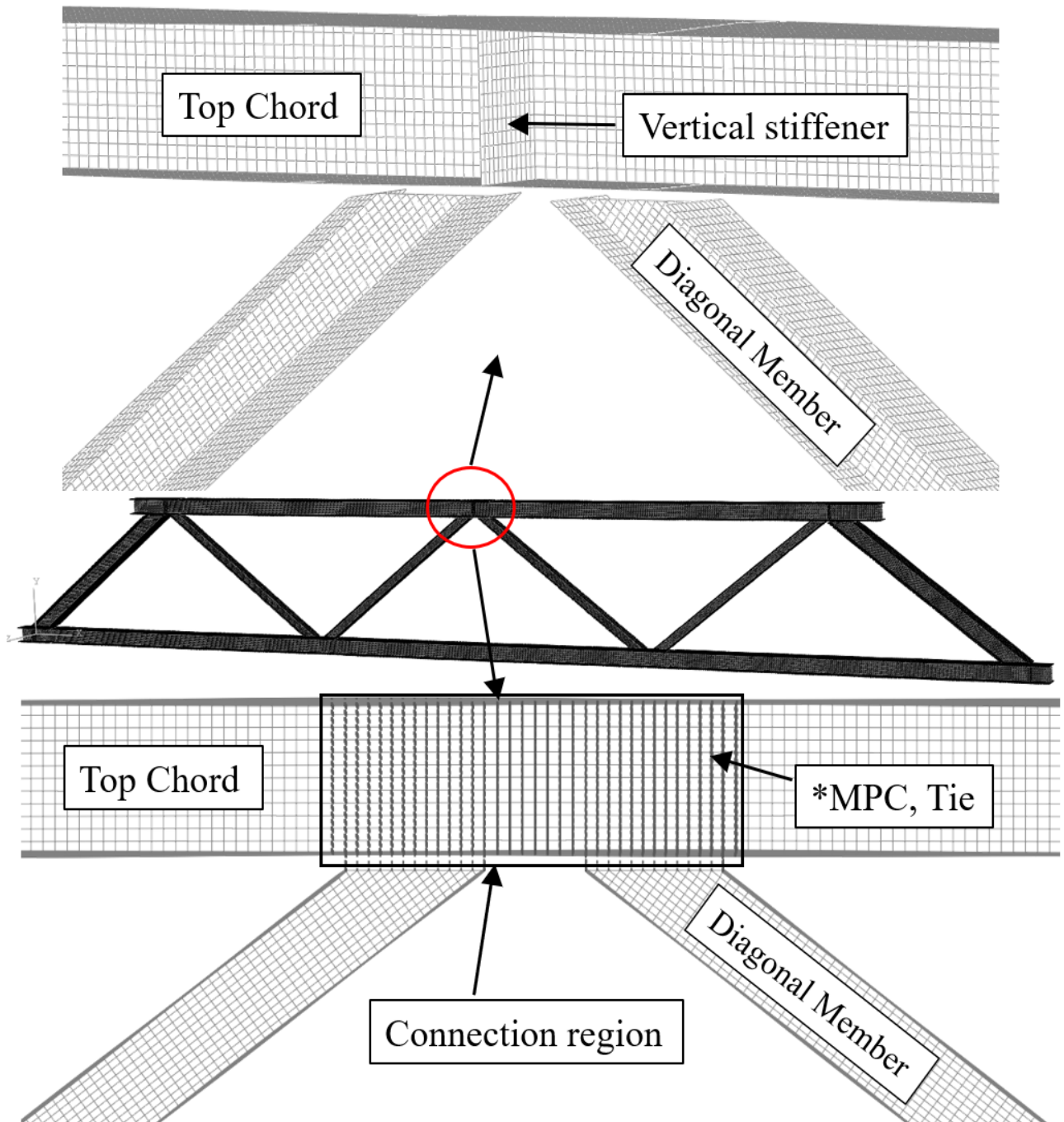


Figure 8: The full rigid connection region in shell FE model

3.2 Beam Finite Element Modelling

As mentioned before, beam FE models are adopted for the proposed advanced analysis with CSM strain limit. Unlike shell FE models, beam FE models can significantly improve the design efficiency by saving plenty time consumed in modelling and computation. Again, FE package Abaqus is adopted to perform the GMNIA analysis using linear Timoshenko B31OS beam element, which is stored in element library of Abaqus for modelling open sections, and 33 section points were assigned along the web and the flange at each cross-section to capture the spread of plasticity accurately. Additionally, the mesh size along the member length should not exceed the maximum value which is equal to the corresponding local buckling half-wavelength $L_{b,cs}$ for the purpose of accurately capturing the full load-deformation response and the spread of plasticity.

Furthermore, the same quad-linear material model is applied again into the beam FE model to account for the effects of material nonlinearity, and then transformed to true stress σ_{true} and strain ε_{true} for Abaqus input. However, the default effective Poisson's ratio for beam element was zero in Abaqus, so a value of 0.5 for the Poisson's ratio needs to be explicitly specified in Abaqus (Walport et al. 2022).

As the CSM strain limit only accounts for the effect of initial geometric imperfections and residual stress at local cross-section level, the initial member imperfection and residual stress are still required to be explicitly defined in the beam FE model. Therefore, the equivalent member bow imperfection for GMNIA listed in Eq. (2.44) were implemented into the beam FE model to reflect the residual stress and member imperfections (Walport et al. 2020).

The comparison between the beam and shell FE models is shown in Fig 9 for a simplified geometry, it is clear to see that the explicitly defined shell elements are now replaced by the predefined beam element in Abaqus. In addition, while this study has already recognized that the finite size of the connection region in the benchmark shell FE model could cause significant effects on the predictive capacity, especially for structural steel truss systems, but the influence of the connection region in the truss system is not the purpose of this study, further improvement may be carried out by replacing the *MPC beam connector by sliced compound cross-section with varying second moment of area I at local cross-section level to represent realistic truss connections. Thus, the results from the GMNIA of beam FE model can then be assessed by the proposed CSM strain limits.

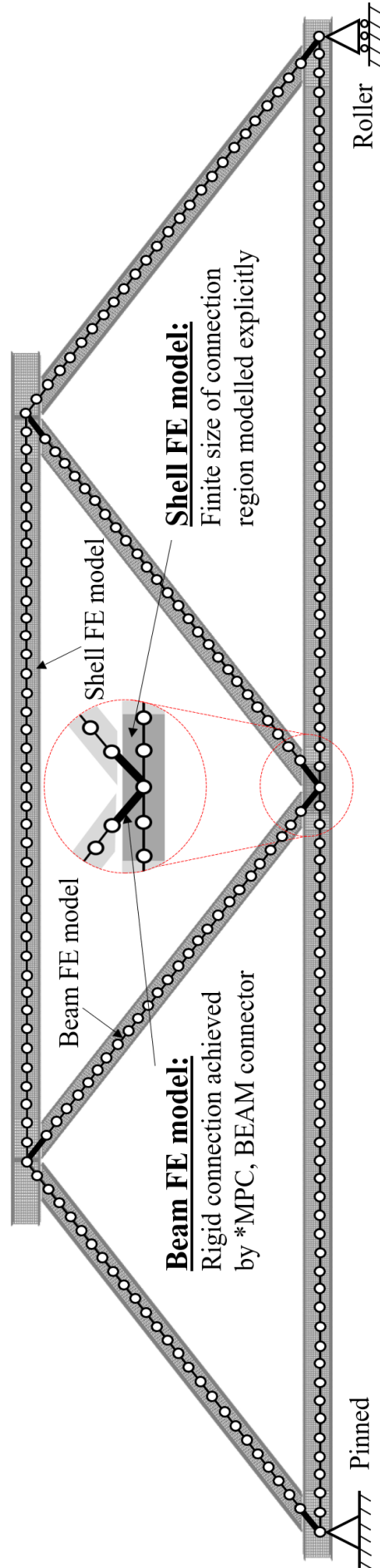


Figure 9: Comparison between the beam and shell finite element model in a simplified truss geometry

4 Results and Discussion

In this section, the accuracy of studied GMNIA-based advanced analysis with CSM strain limits for I-section trusses is evaluated. For the Benchmark shell model, the ultimate resistance is simply taken as the maximum load when the load deformation response decreases, and the ultimate resistance generated from the beam FE model with strain limit check is taken as the lower of (1) the peak load at which the maximum load is reached at structure failure or (2) the load when the averaged longitudinal compressive strain ε_{Ed} over the elastic local buckling half-wavelength $L_{b,cs}$ has reached the determined CSM strain limit ε_{csm} or $\rho_{csm}\varepsilon_{csm}$. Meanwhile, the ultimate resistance generated by the simplified beam FE models with cross-section capacity check are taken as the lower of the peak load or the load occurred when the section capacity check (Eq. (2.37)) cannot be satisfied anymore. However, due the varying load increments in nonlinear analysis, the exact load factor at which the strain limit or maximum C-S capacity is reached will normally not match the solution point obtained from Abaqus, interpolation between the load levels at either side of the solution point is thus required to increasing the result accuracy, the analysis procedures of each method are shown in the following Fig 10. Furthermore, the capacity predictions obtained from each analysis method will be compared against the benchmark result respectively.

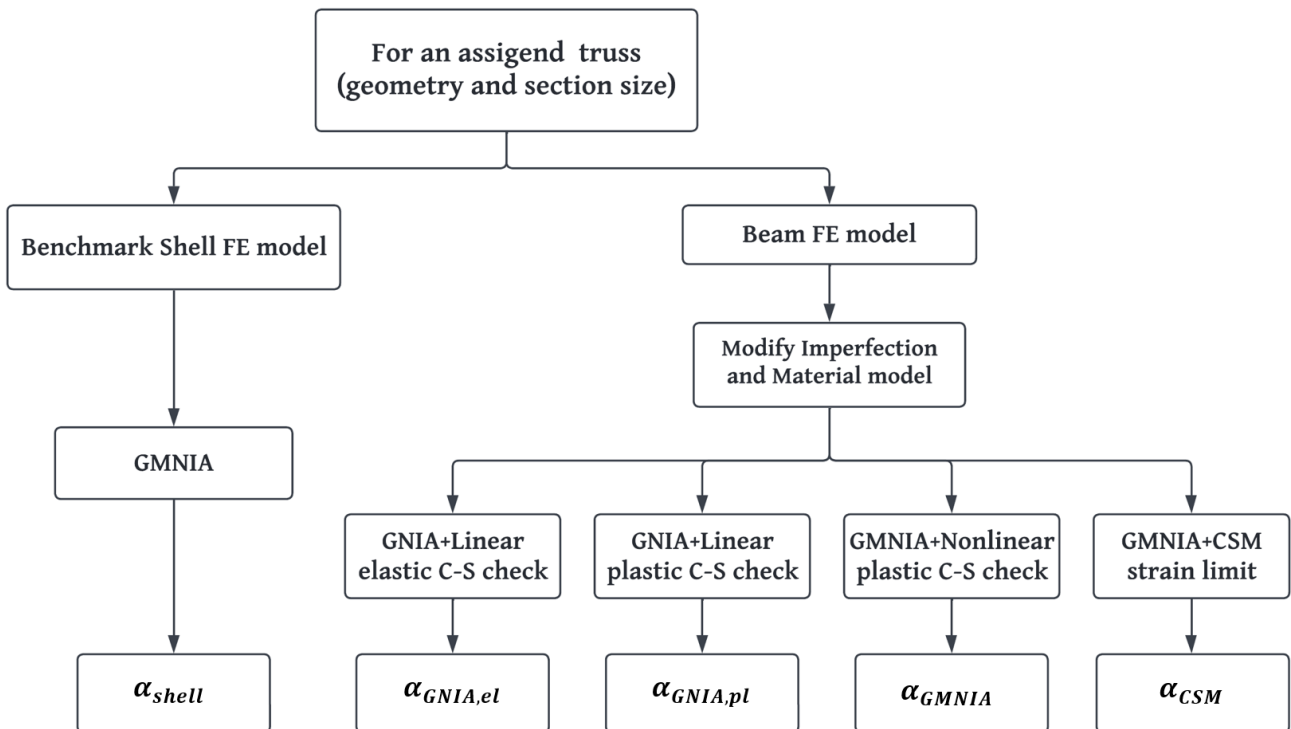


Figure 10: Analysis procedures for different type of analysis mentioned in Section 2

4.1 Case Study

To validate the accuracy of each generated FE model, the comparison is firstly carried out for a truss with trial geometry and random member sizes, the geometry and section size selection is based on avoiding the occurrence of overlapping, the section sizes and truss geometry are given as below.

Table 3: Section sizes for the truss analyzed in Case 1

Chord	Diagonal Member
356×406 × 340	305×305 × 118

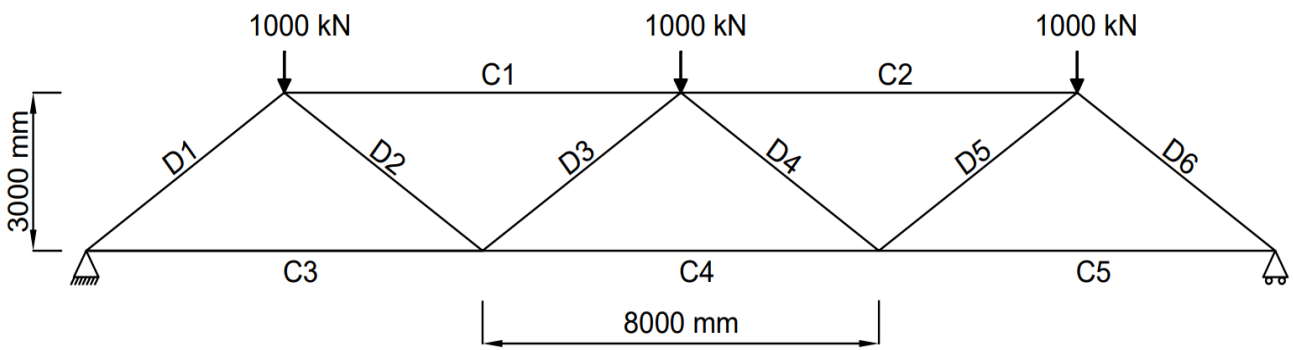


Figure 11: Truss geometry, loading and support conditions for Case 1

Figure 12 depicts the load-deformation curves of the shell FE model and the beam FE model, the deformation u is extracted at the point where the second point load is applied. It can be seen that the initial stiffness (α/u) are identical between the benchmark shell FE model and the beam FE model during the elastic loading period, this phenomenon could represent that the applied equivalent bow imperfection in the beam FE model can simulate similar second order effect as the residual stress and the initial member out-of-straightness applied in the shell FE model. In contrast, the identical stiffness during elastic loading period also means that the shell FE model successfully approximated the fully rigid connection area in the beam FE model. Additionally, both models successfully predicted that the failure point would occur at the middle part on the right sided diagonal, the comparison of the failure point between both models is shown in Fig 13.

Table 4: Comparisons between the ultimate resistance α_{Shell} of the benchmark shell model, the studied advanced analysis method α_{CSM} and other considered advanced analysis (Case 1)

Type of analysis	Ultimate resistance (Load Factor)	Normalised ratio ($\alpha_{Shell}/\alpha_{Analysis}$)
Benchmark shell FE model (GMNIA)	2.070	1
CSM strain limits (GMNIA)	2.036	0.984
Nonlinear plastic C-S check (GMNIA)	2.017	0.974
Linear elastic C-S check (GNIA)	1.981	0.957
Linear plastic C-S check (GNIA)	1.931	0.932
Traditional design approach	1.852	0.895

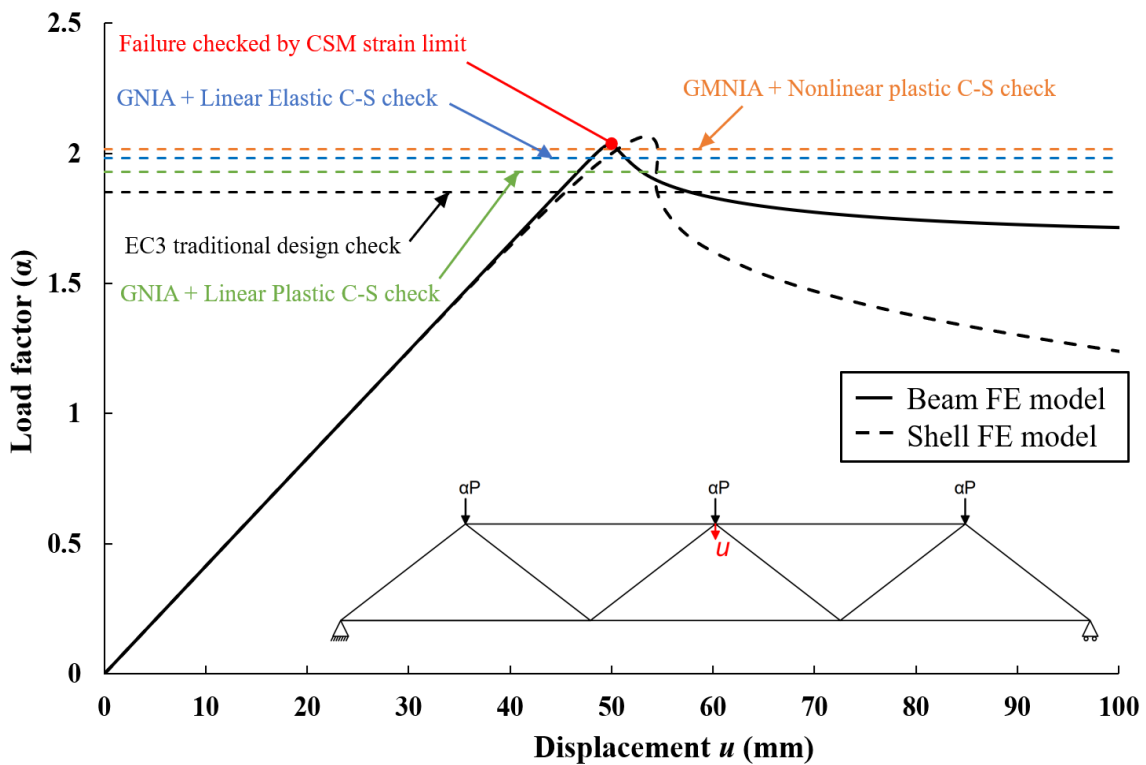


Figure 12: Load-deflection paths and predicted ultimate resistances for Case 1

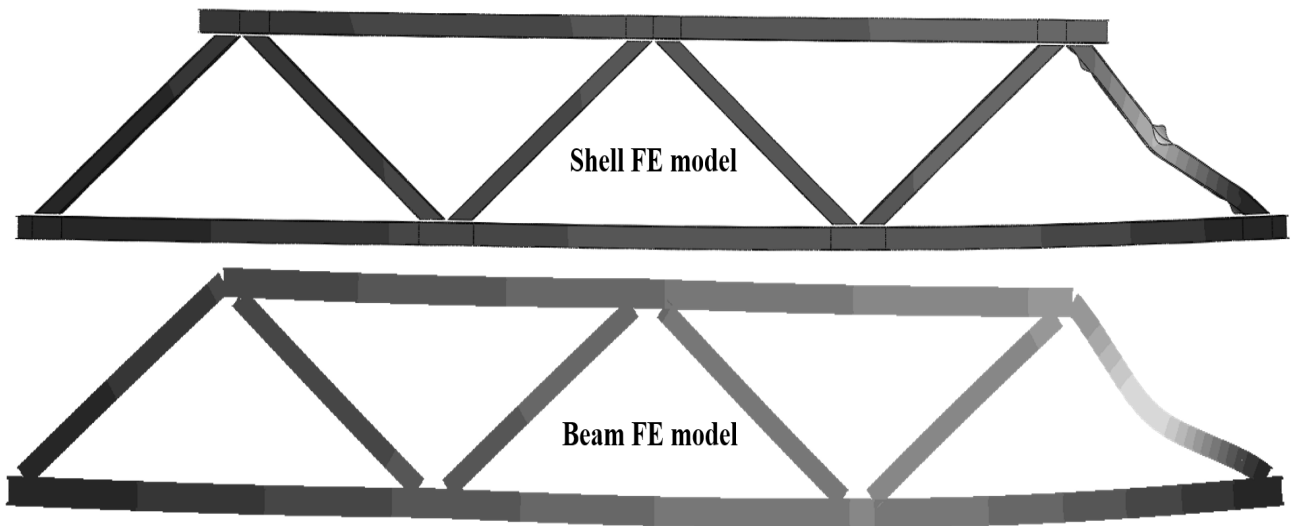


Figure 13: Comparison of failure point between shell FE mode and beam FE model for Case 1

From Fig 12 and Table 4, it is clear to see that the ultimate capacity predicted by traditional design approach is relatively conservative comparing to other advanced analysis methods, and there is an approximately 10 percent increment in the ultimate capacity prediction for the benchmark shell FE model compared to the traditional design approach. Furthermore, All the advanced analysis methods predicted a relatively lower ultimate capacity than the benchmark result, which means the safety of the design is ensured while saving the material cost, the studied advanced analysis with CSM strain limit predicted the closest ultimate capacity to the benchmark result among all the advanced analysis using beam FE models. In reality, the I-section truss are assembled together with individual members by means of gusset plates, and the gusset plate is normally covered on to individual members for a certain distance, so the traditional design approach could use lower effective length to increase the flexural buckling resistance. For instance, the ultimate capacity predicted by traditional method can be increased to $\alpha = 1.95$ by using $0.9 L_{cr}$. However, this method may only applicable to limited trusses, as this tested truss only represents a single member failure rather than the truss acting as a completed structure, and this phenomenon will be further discussed in the following cases.

In addition, it is noted that the ultimate capacity predicted by the studied CSM strain limit method is governed by the peak load during the loading history rather than calculated strain limit. In order to investigate under what circumstances the ultimate capacity is most likely to be governed by the CSM strain limits, the case study has been carried out for multiple

truss systems with various geometry and various section size, and the results are rearranged in a relationship between local cross-section slenderness $\bar{\lambda}_p$ and member slenderness $\bar{\lambda}$ shown in Fig 14.

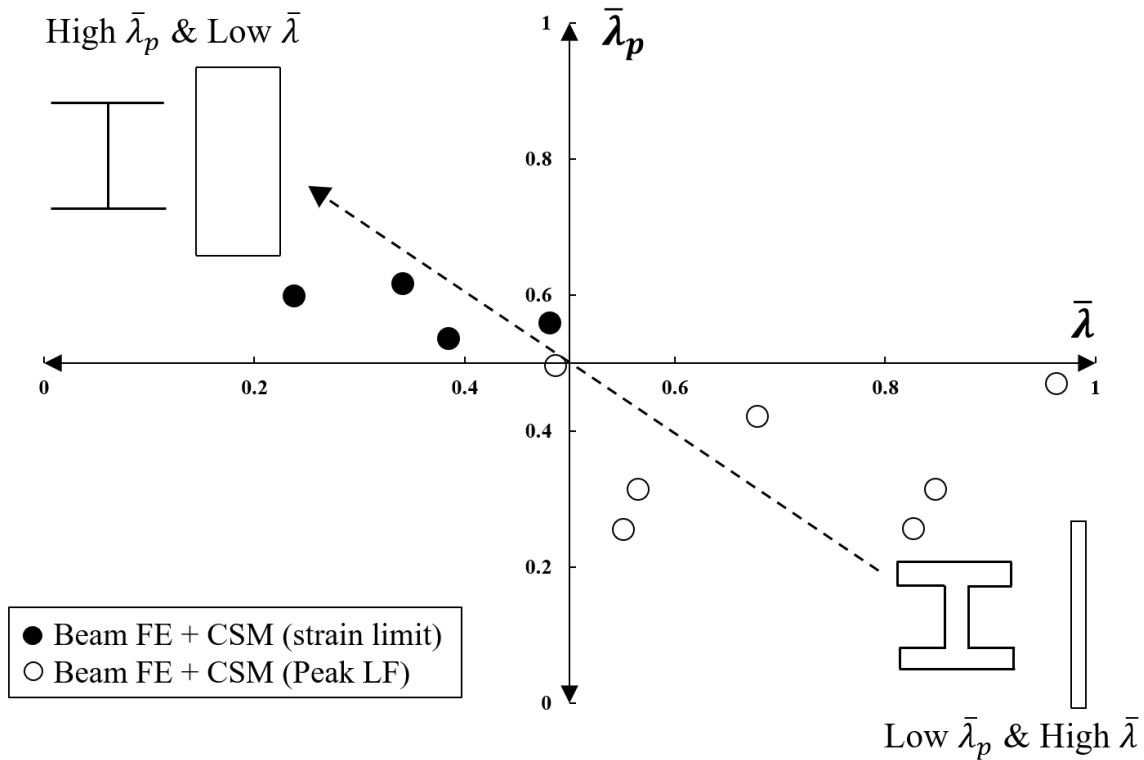


Figure 14: Investigation about the CSM strain limit governed cases

In Fig 14, the solid circle is representing those truss systems which the ultimate capacity is governed by CSM strain limit, and the empty circle is representing those cases governed by the peak load during the loading history. Although the simulated results are not yet sufficient to draw a conclusion about this phenomenon, but it is clear to see that the CSM strain limit is more likely to govern these members which is 'slender' in cross-section (high $\bar{\lambda}_p$) but relatively 'stocky' in member (low $\bar{\lambda}$), at least for these type of simple Warren trusses.

For a more visual representation of CSM strain limit governed cases, a modified truss system based on the presented case 1 is shown below in Fig 15. Note, the section sizes are the same as shown in Table 3, but the thickness of the flange and web has been reduced for 1mm in diagonal members to achieve 'slender' cross-section, and the size of the truss has been equally scaled down to half of the original size to achieve 'stocky' member.

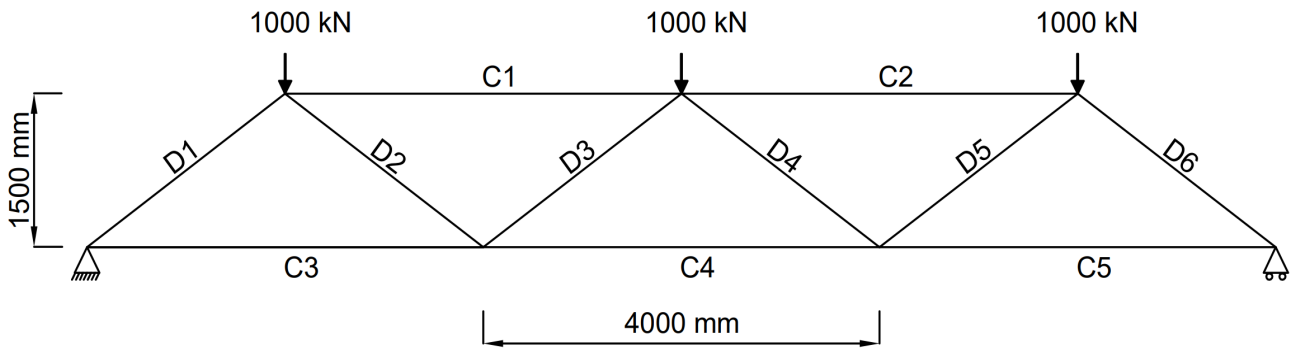


Figure 15: Truss geometry, loading and support conditions for Case 2

The predicted ultimate capacity of the modified truss (Case 2) is reported in following Table 5, and the load-displacement curve extracted from the beam FE model and the shell FE model are given in Fig 17. For this case, both shell FE model and beam FE model presented a continuous capacity strength increase after the first member buckled, this may well explained by Fig 16, the bottom chord started to carrying a greater amount of force and moment since the right sided diagonal member has buckled, but the shell FE model will essentially fail at a lower load factor. Additionally, the ultimate capacity in the beam FE model is detected at the first instance when the averaged longitudinal compressive strain ε_{Ed} has reached the determined CSM strain limit ε_{CSM} at local cross-section level. The ultimate capacity determined from studied CSM strain limit method remains the closest to the benchmark result, consistently benefits a 10 percent capacity increment comparing to traditional design approach, while those ultimate capacity generated using second order elastic analysis methods are very close to the traditional design approach, with the linear elastic C-S check (GNIA) in particular is relatively conservative. Furthermore, the application of a reduced $0.9 L_{cr}$ effective length would make other methods more conservative in this case.

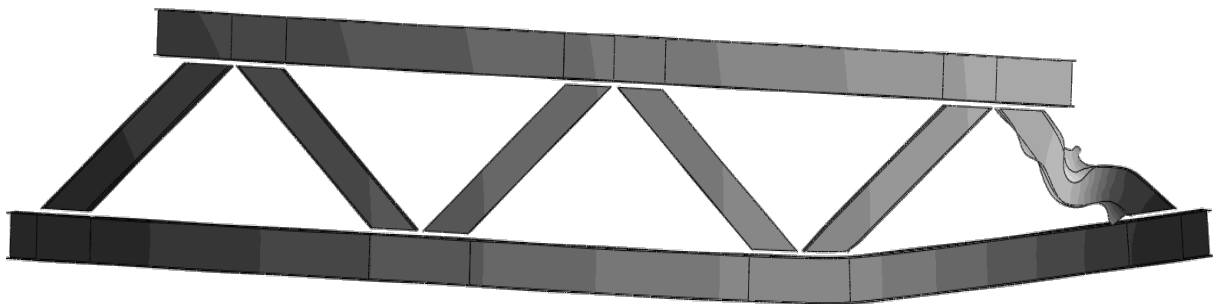


Figure 16: deformed shape for Case 2 truss from shell FE model

Table 5: Comparisons between the ultimate resistance α_{Shell} of the benchmark shell model, the studied advanced analysis method α_{CSM} and other considered advanced analysis (Case 2)

Type of analysis	Ultimate resistance (Load Factor)	Normalised ratio ($\alpha_{Shell}/\alpha_{Analysis}$)
Benchmark shell FE model (GMNIA)	1.924	1
CSM strain limits (GMNIA)	1.904	0.990
Nonlinear plastic C-S check (GMNIA)	1.775	0.922
Linear elastic C-S check (GNIA)	1.713	0.890
Linear plastic C-S check (GNIA)	1.739	0.904
Traditional design approach	1.720	0.894

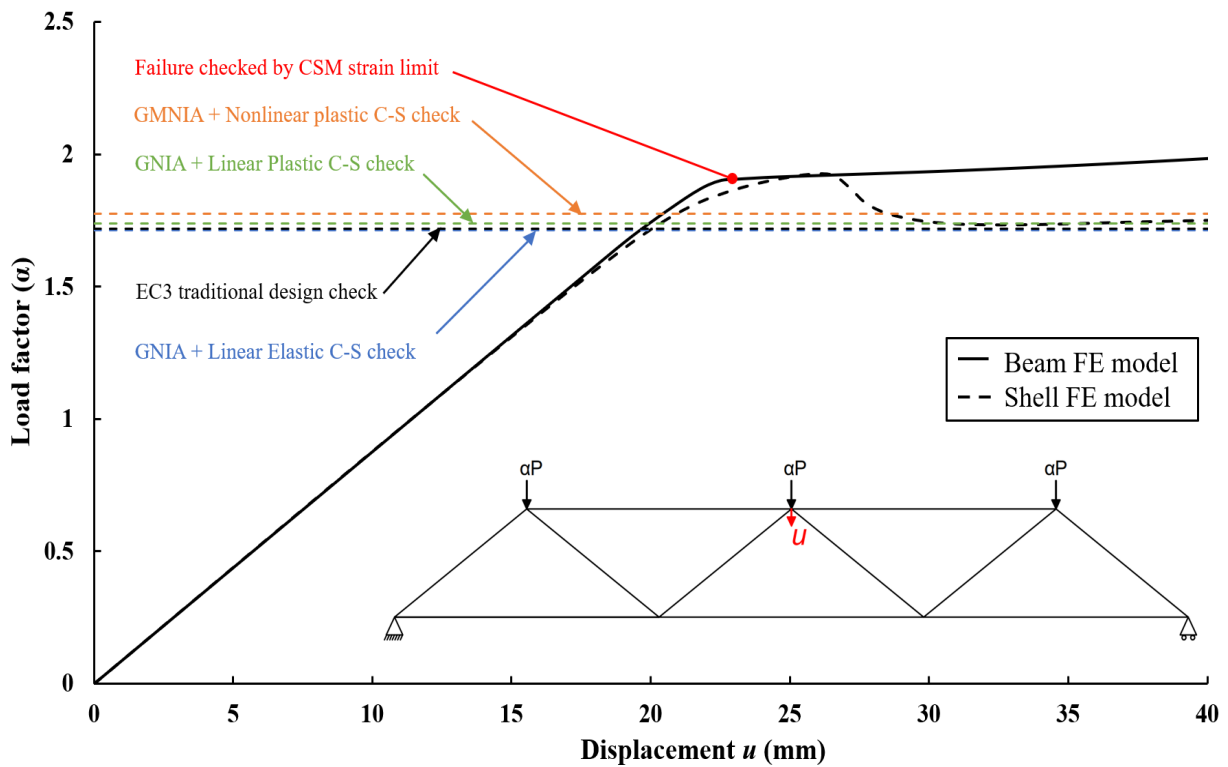


Figure 17: Load-deflection paths and predicted ultimate resistances for Case 2

In these previous cases, the same section size has been assigned to all the diagonal members for simplicity purpose. In order to apply the studied advanced analysis with CSM strain limit into truss design, the sizes of each individual member has to be assigned separately which means each individual member will be allocated a different section accordingly. To validate the modified FE model with multiple section sizes in the truss, the same geometry used in Case 1 is adopted, but the most heavily loaded diagonal members have been randomly assigned a bigger section, while smaller section is selected for those internal diagonal members, the selected section sizes can be found in the following Table 6.

Table 6: Section sizes for the truss analyzed in Case 3

Chord Member	Internal Diagonal Member	Side Diagonal Member
356×406 × 340	203×203 × 118	356×406 × 340

Comparing to the deformed shape generated by the reference shell FE model and beam FE model in Fig 18, both models are applicable for the truss consists multiple section sizes, and both models captured the failure member correctly, it is clear to see that buckling occurred in the internal member would influence the overall structural response, the truss is now behaving more like a group. From the ultimate capacity comparisons shown in Table 9 and Fig 19, it is not surprising to see that the CSM strain limit method still ranked as the most sustainable design method, and the ultimate resistance increment is about 15 percent in this case compared to the traditional design method. Comparing to these conservative methods based on GNIA, the nonlinear plastic C-S check (GMNIA) take the benefits from material non-linearity (strain hardening) by using the quad-linear material model.

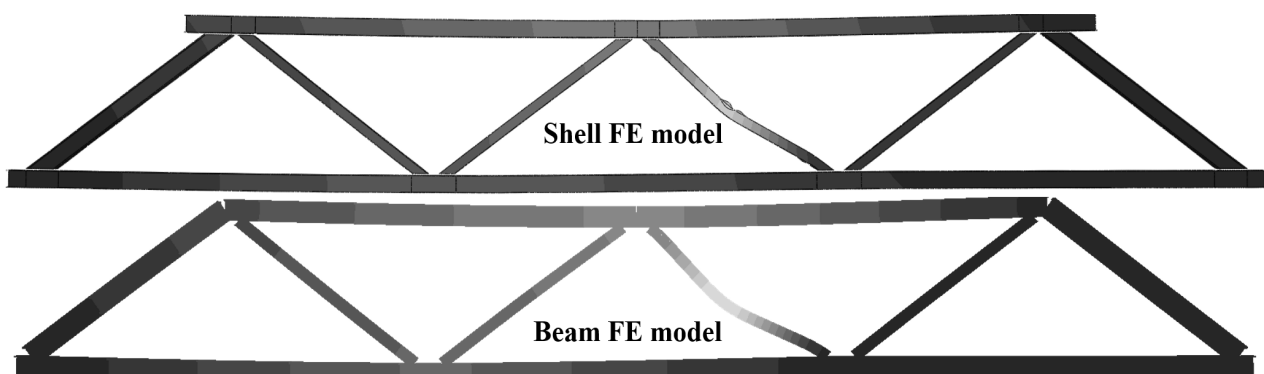


Figure 18: Comparison of failure point between shell and beam FE model for Case 3

Table 7: Comparisons between the ultimate resistance α_{Shell} of the benchmark shell model, the studied advanced analysis method α_{CSM} and other considered advanced analysis (Case 3)

Type of analysis	Ultimate resistance (Load Factor)	Normalised ratio ($\alpha_{Shell}/\alpha_{Analysis}$)
Benchmark shell FE model (GMNIA)	3.591	1
CSM strain limits (GMNIA)	3.464	0.965
Nonlinear plastic C-S check (GMNIA)	3.322	0.925
Linear elastic C-S check (GNIA)	2.931	0.816
Linear plastic C-S check (GNIA)	2.840	0.791
Traditional design approach	2.920	0.813

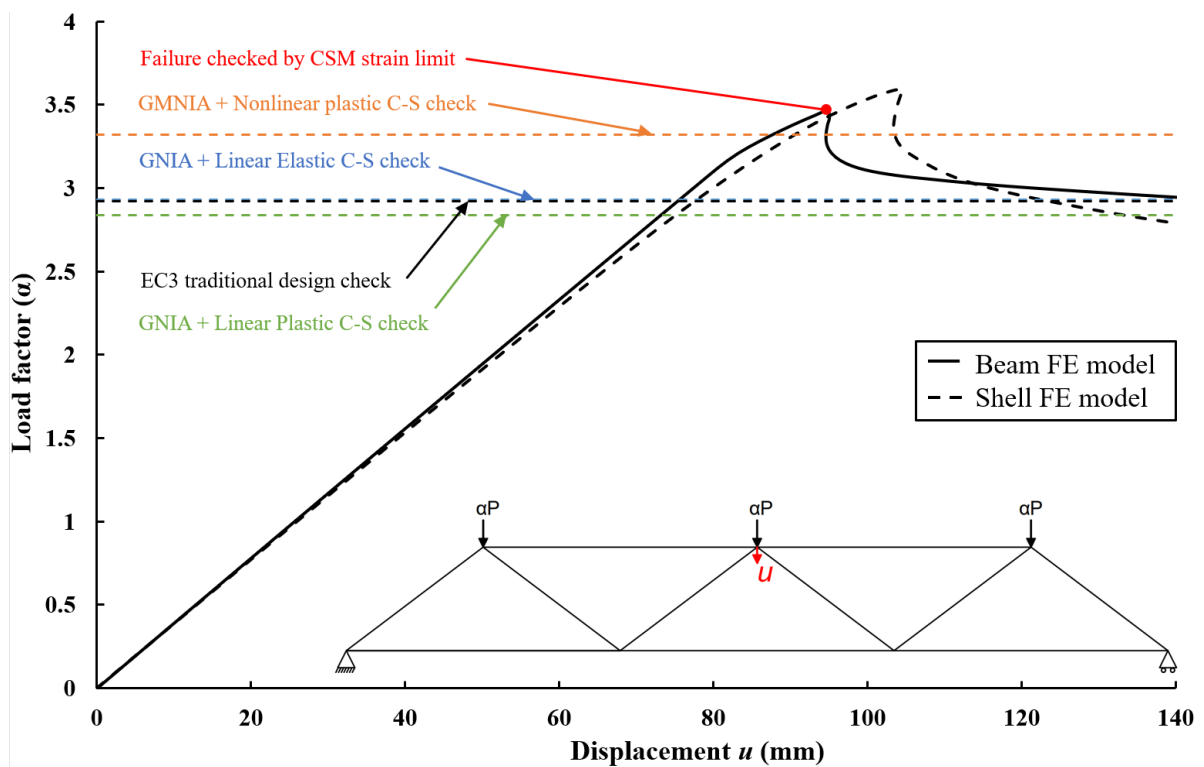


Figure 19: Load-deflection paths and predicted ultimate resistances for Case 3

4.2 Design of Warren Truss

As mentioned before, the section sizes in Case 1, Case 2 and Case 3 are randomly assigned. In order to apply the studied advanced analysis with CSM strain limit into practical truss design, each individual member has been sized separately for the given truss geometry and loading conditions shown in Fig 20, the internal force is firstly determined from first order global analysis (force equilibrium), and the sections are then sized according to the conventional design approach stated in prEN 1993-1-1, are the selected sections are shown in Table 9.

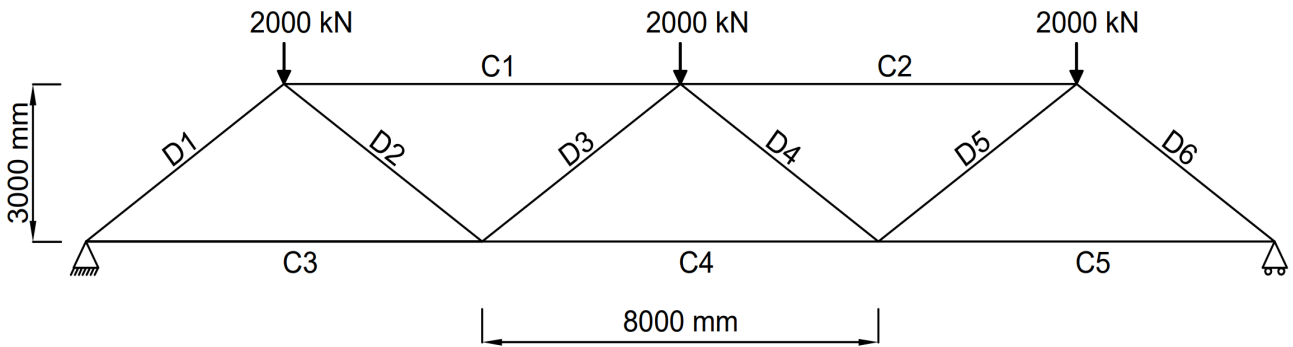


Figure 20: Truss geometry, loading and support conditions (Case 4)

Table 8: Section sizes for the truss analyzed in Case 4

Chord Member	Internal Diagonal Member	Side Diagonal Member
305×305 × 198	203×203 × 52	356×305 × 137

For the designed warren truss consists 3 different sized sections, the second order elastic analysis methods are relatively underestimated the ultimate resistance comparing to the traditional design approach. As the cross-section check is mainly governed by the interaction between compressive force and bending moment, the different sized cross-sections will result different rotational capacity in each individual member, so the generated greater amount of bending moment will lead to those methods using C-S check yields at a lower limit. Additionally, as preferred advanced analysis method, the CSM strain limit method consistently yielded at a upper limit comparing to all the other advanced analysis methods (only 1.6% lower than the benchmark result), while the predicted ultimate capacity is still on the safe side for all investigated cases.

Table 9: Comparisons between the ultimate resistance α_{shell} of the benchmark shell model, the studied advanced analysis method α_{CSM} and other considered advanced analysis (Case 4)

Type of analysis	Ultimate resistance (Load Factor)	Normalised ratio ($\alpha_{shell}/\alpha_{Analysis}$)
Benchmark shell FE model (GMNIA)	1.203	1
CSM strain limits (GMNIA)	1.183	0.984
Nonlinear plastic C-S check (GMNIA)	1.093	0.908
Linear elastic C-S check (GNIA)	1.001	0.832
Linear plastic C-S check (GNIA)	0.983	0.818
Traditional design approach	1.076	0.894

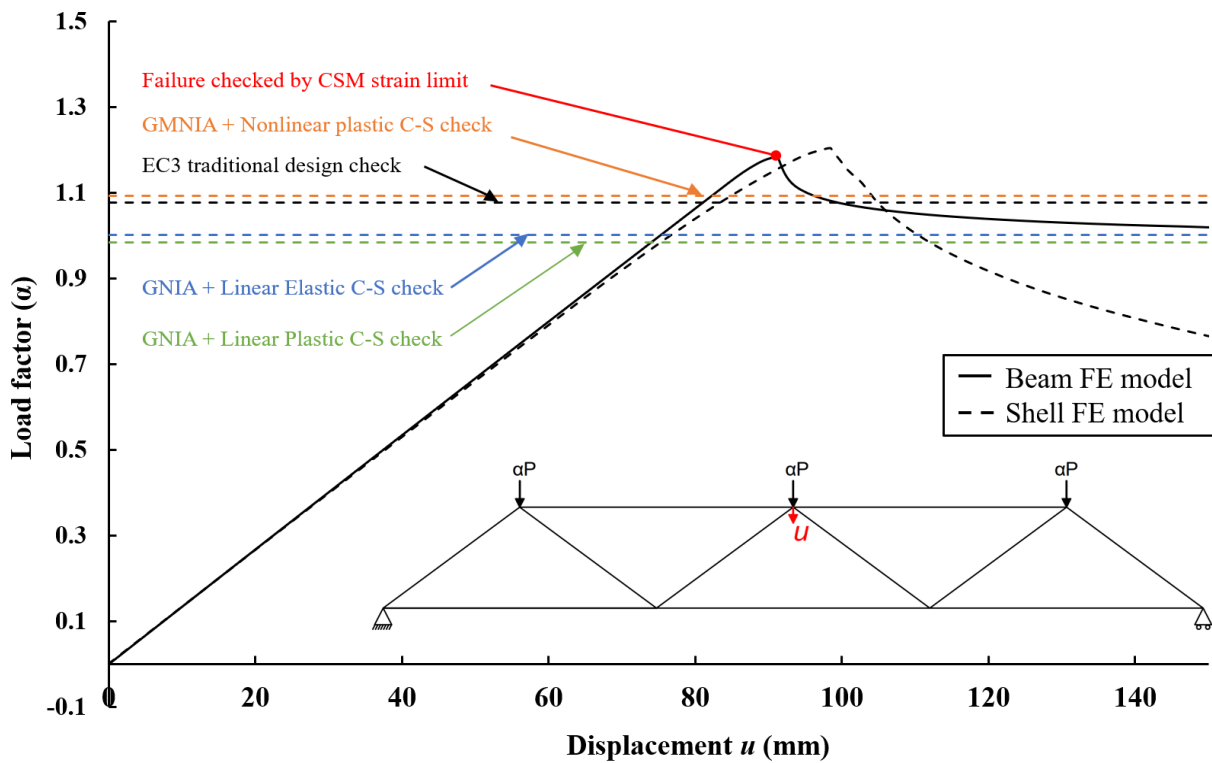


Figure 21: Load-deflection paths and predicted ultimate resistances for Case 4

5 Worked Example

For illustration purpose, a worked example using mentioned analysis methods (Section 2) is presented in this section, the worked example considers a simple hot-rolled steel truss system, the truss geometry, support conditions and design loading can be found in following Fig 22. The steel truss is full restricted at out-of-plane deformation, so the worked example is only considering in-plane failure types, and the following calculations are all based on centreline dimensions, the section size of each member can be found in the following Table 10.

Table 10: Section sizes for the truss shown in worked example

Chord	Diagonal Member
356×406 × 340	305×305 × 97

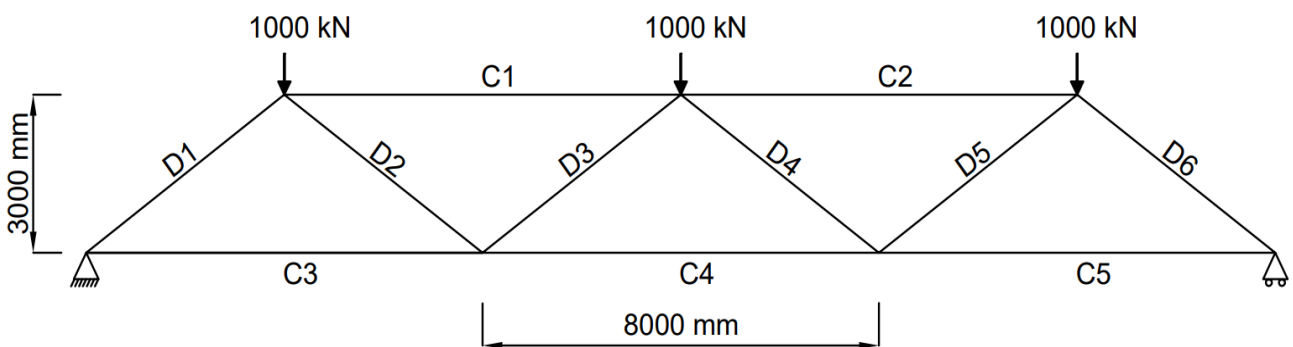


Figure 22: Truss geometry, loading and support conditions for worked example

(1) Traditional Design Check

The first step in traditional design check is to determine the internal forces by carrying out a first order global analysis (force equilibrium), the determined internal forces for the assigned truss geometry is shown in Fig 23.

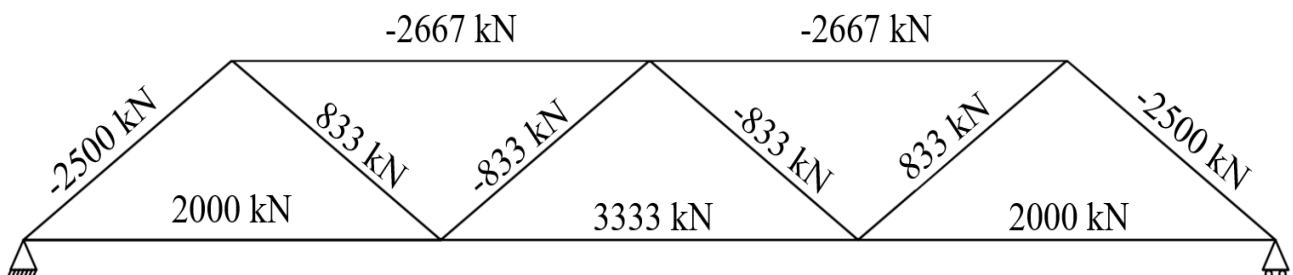


Figure 23: Internal forces determine from first order global analysis

In above Fig 23, the negative sign is indicating compressive force, and positive sign is representing tension force.

Following the method of cross-section classification provided in prEN 1993-1-1, both sections can be classified as Class 1 cross-section, and the section properties satisfied the requirement of using buckling curve b for y-y axis, so the imperfection factor α is taken as 0.34. Therefore, the buckling reduction factor χ for the most critical compression members can thus be calculated by using Eq. (2.3 - 2.6), χ is equal to 0.890 for the 5m compressive diagonal member and 0.826 for the compressive chord member with 8m long, the member flexural buckling resistance are given by:

$$N_{b,Rd} = \frac{\chi Af_y}{\gamma_{M1}} = 3880kN \quad \text{for the 5m compressive diagonal member}$$

$$N_{b,Rd} = \frac{\chi Af_y}{\gamma_{M1}} = 12100kN \quad \text{for the 8m compressive chord member}$$

In addition, the tension resistance of the assigned two cross-sections are given by:

$$N_{pl,Rd} = \frac{Af_y}{\gamma_{M0}} = 4366.5kN \quad \text{for } 305 \times 305 \times 97$$

$$N_{pl,Rd} = \frac{Af_y}{\gamma_{M0}} = 15371.5kN \quad \text{for } 356 \times 406 \times 340$$

From the above resistance calculations and Fig 23, it is clear to see that the most critical members are the side diagonals (D1 and D6) which are subjected in compression, the load factor α_{LA} can thus be calculated as below:

$$\alpha_{LA} = \frac{N_{b,Rd}}{N_{Ed}} = \frac{3880kN}{2500kN} = 1.552$$

The load factor α_{LA} indicates the number of times the structure can withstand the current applied load (1000kN) using the conventional design approach stated in prEN 1993-1-1, this load factor will be further compared with other analysis methods.

(2) GMNIA + CSM strain limit

As previously explained in Section 2, the maximum averaged compressive strains must be less than the respective CSM strain limit in all cross-sections of the structure, once the average compressive strain of a single cross-section reaches the CSM strain limit, the structure will be defined as failed. For simplicity purpose, only the calculation procedures for the critical cross-section is presented.

The first step is to calculate the full cross-section local buckling stress $\sigma_{cr,cs}$ using the first order elastic stress distribution taken from Abaqus shown in Fig 24.

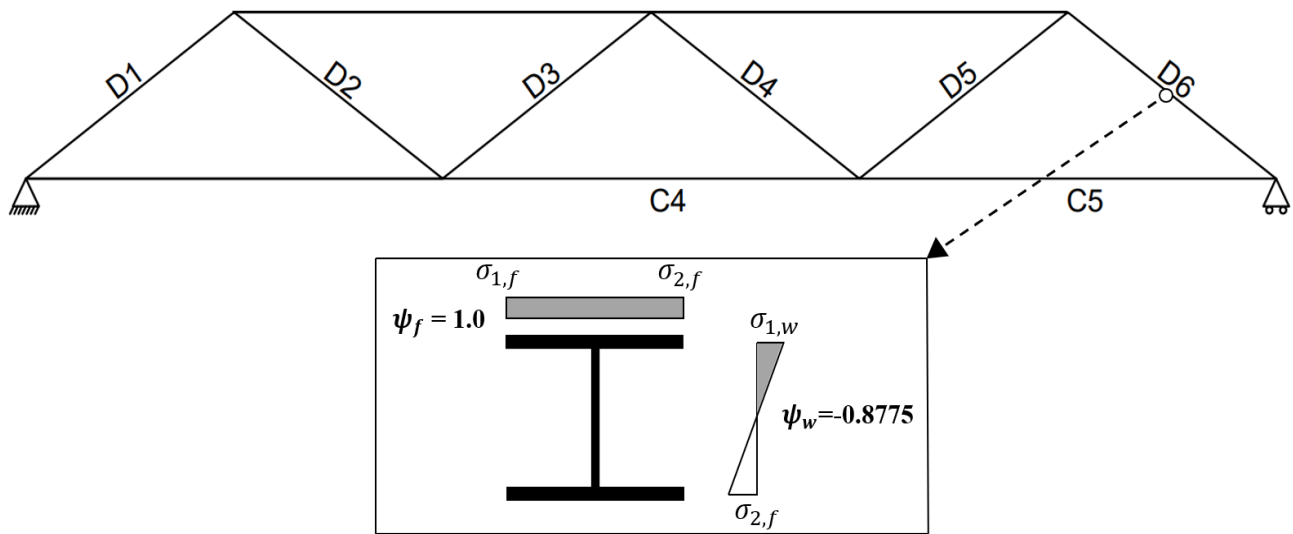


Figure 24: The elastic stress distribution at the critical cross-section

As the compression flange is uniformly compressed at the critical section ($\psi_f = 1.0$), so the buckling coefficient for the isolated outstand flanges with simply-supported and fixed boundary conditions can be simply taken as:

$$k_f^{SS} = 0.43 \quad \& \quad k_f^F = 1.25$$

For the internal web subjected to combined bending and compression with $\psi_w = 0.8775$, which is taken from the 5_{th} step during elastic loading at element 2195 (critical section), the buckling coefficient are given as below:

$$k_w^F = \frac{14.29}{1.05 + \psi} = \frac{14.29}{1.05 + 0.8775} = 7.414$$

$$k_w^{SS} = \frac{8.2}{1.05 + \psi} = \frac{8.2}{1.05 + 0.8775} = 4.254$$

The corresponding elastic critical buckling stresses can thus be calculated using Eq. (2.16) respectively:

$$\sigma_{cr,f}^{SS} = k_f^{SS} \frac{\pi^2 E}{12(1-\nu^2)} \left(\frac{t_f}{c_f} \right)^2 = 830.64 \text{MPa} \quad \sigma_{cr,f}^F = k_f^F \frac{\pi^2 E}{12(1-\nu^2)} \left(\frac{t_f}{c_f} \right)^2 = 2414.65 \text{MPa}$$

$$\sigma_{cr,w}^{SS} = k_w^{SS} \frac{\pi^2 E}{12(1-\nu^2)} \left(\frac{t_w}{c_w} \right)^2 = 924.94 \text{MPa} \quad \sigma_{cr,w}^F = k_w^F \frac{\pi^2 E}{12(1-\nu^2)} \left(\frac{t_w}{c_w} \right)^2 = 1611.79 \text{MPa}$$

As the maximum compressive stresses in the flange and web are identical, so the correction factors β_f and β_w are taken as 1, and the upper and lower bound to the full cross-section local buckling stress can then be derived from Eq. (2.15)

$$\sigma_{cr,p}^F = \min(\beta_f \sigma_{cr,f}^F, \beta_w \sigma_{cr,w}^F) = 1611.79 \text{MPa}$$

$$\sigma_{cr,p}^{SS} = \min(\beta_f \sigma_{cr,f}^{SS}, \beta_w \sigma_{cr,w}^{SS}) = 830.64 \text{MPa}$$

In addition, the interaction coefficient ζ is then calculated using Eq. (2.17 & 2.20):

$$\phi = \frac{\sigma_{cr,f}^{SS}}{\sigma_{cr,w}^{SS}} = 0.898$$

$$\zeta = 0.15 \frac{t_f}{t_w} \phi = 0.2095 \geq \frac{t_w}{t_f} (0.4 - 0.25\phi) = 0.1062$$

Thus, the elastic local buckling stress of the full cross-section at the critical element can be calculated from Eq. (2.12).

$$\sigma_{cr,cs} = \sigma_{cr,p}^{SS} + \zeta (\sigma_{cr,p}^F - \sigma_{cr,p}^{SS}) = 830.64 + 0.2095(1611.79 - 830.64) = 994.368 \text{Mpa}$$

For the critical cross-section, the local cross-section slenderness $\bar{\lambda}_p$ can then be calculated using Eq. (2.11).

$$\bar{\lambda}_p = \sqrt{\frac{f_y}{\sigma_{cr,cs}}} = \sqrt{\frac{355}{994.368}} = 0.5975$$

Hence, the normalised GSM strain limit for the cross-section under consideration can be calculated using Eq. (2.9) as the local cross-sectional slenderness $\bar{\lambda}_p$ is less than 0.68.

$$\frac{\varepsilon_{csm}}{\varepsilon_y} = \frac{0.25}{\bar{\lambda}_p^{3.6}} = \frac{0.25}{0.5875^{3.6}} = 1.5963$$

Note that this calculated CSM strain limit might not be the final value, additional shear capacity check is required in case of high shear.

$$V_{pl,Rd} = \frac{A_v (f_y / \sqrt{3})}{\gamma_{M0}} = 674.7 \text{ kN}$$

As a result, no further adjustment is required on the calculated CSM strain limit since the shear force at the critical section is relatively small comparing to the plastic shear capacity.

Furthermore, the calculated buckling half-wavelengths of isolated plates by using Eq. (2.31) are $L_{b,w}^{SS} = 292.50$ mm, $L_{b,w}^F = 193.05$ mm, $L_{b,F}^{SS} = 716.50$ mm and $L_{b,f}^F = 251.87$ mm. Using Eq. (2.32 & 2.33), the upper limit and the lower limit to the cross-section local buckling half-wavelength are $L_{b,p}^{SS} = 691.34$ mm and $L_{b,p}^F = 248.39$ mm, the elastic local buckling half-wavelength $L_{b,cs}$ of the full cross-section can thus be calculated using the interaction coefficient determined for elastic local buckling stress:

$$L_{b,cs} = L_{b,p}^{SS} - \zeta (L_{b,p}^{SS} - L_{b,p}^F) = 598.56 \text{ mm} \quad (5.1)$$

In Fig 26, the CSM strain limit ε_{CSM} is then checked with the averaged strain $\varepsilon_{Ed,av}$ over the elastic local buckling half-wavelength $L_{b,cs}$. The failure is found at load step 39 in diagonal member 6, the ultimate resistance α_{CSM} is found to be 1.673 which is occurred before the peak load.

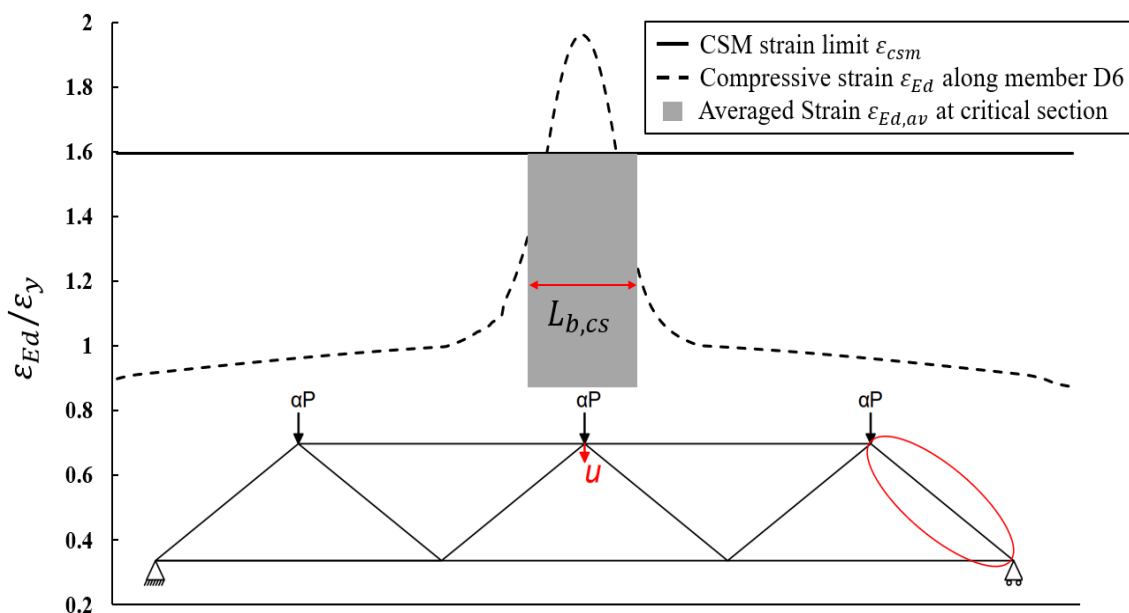


Figure 25: Strain distribution along the diagonal member 6

(3) GMNIA + Nonlinear Plastic C-S check

As mentioned before, the same beam FE model used for CSM strain limit check is also adopted here for the second order inelastic analysis with C-S check (Section 2.3.2). By utilizing Eq. (2.39) to Eq. (2.43) for the nonlinear plastic moment capacity calculation and the extracted design moment and axial force from Abaqus, the ultimate resistance of the assigned truss system can be easily determined from the critical cross-section, the following Fig 27 is representing the relationship between the internal force-moment distribution and the corresponding cross-section capacities at the critical element.

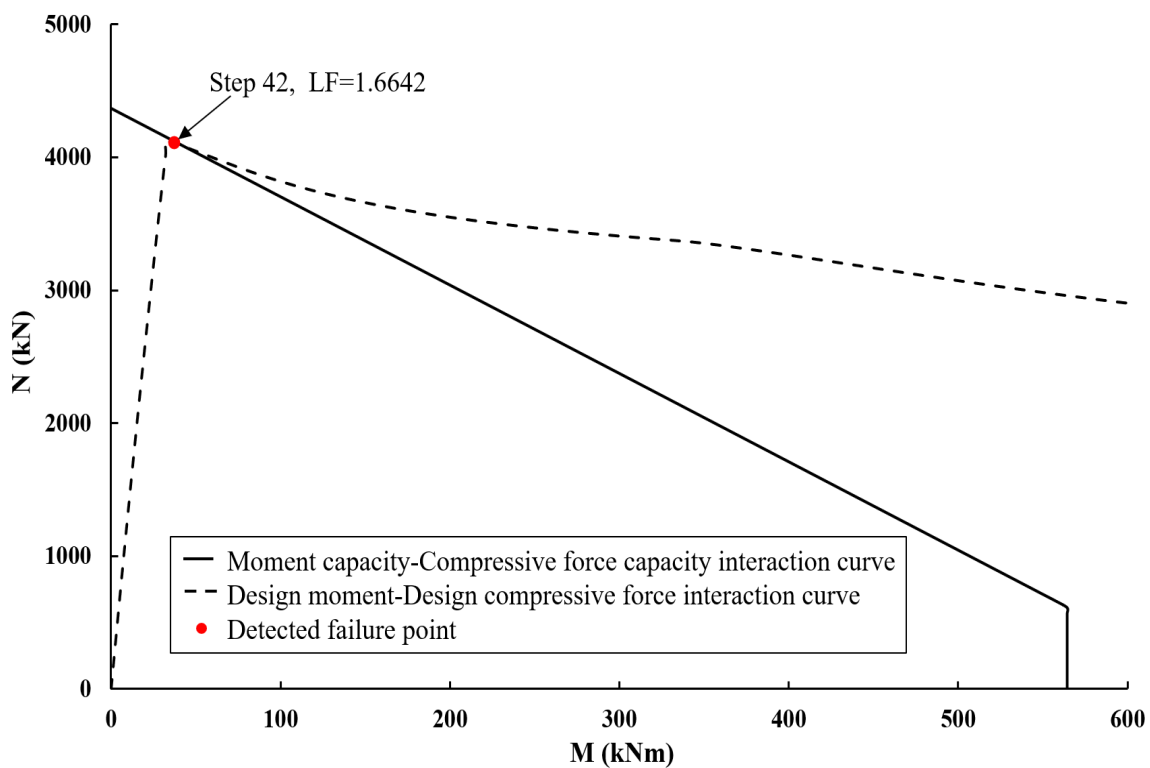


Figure 26: GMNIA with nonlinear plastic cross-section check

It is clear to see that the design moment-Compressive force interaction curve crosses the M-N capacity interaction curve at the 42th step during the loading history in Abaqus, so the ultimate capacity α_{GMNIA} using nonlinear plastic C-S check can be directly taken as the load factor at 42th step.

$$\alpha_{GMNIA} = LF (42_{th} \text{ step}) = 1.6642$$

(4) GNIA + Linear elastic C-S check

The beam FE model used for GNIA analysis is simplified based on the previous beam FE model by replacing the quad-linear material model with a perfect elastic material model, and the equivalent bow imperfection has also been modified for elastic cross-section verification according to prEN 1993-1-1 shown in Table 1. Additionally, the cross-section capacity is checked using Eq. (2.37) at each section, but the bending moment capacity is calculated based on the corresponding elastic modulus W_{el} , the linear elastic cross-section check for the critical section is shown in the following Fig 27.

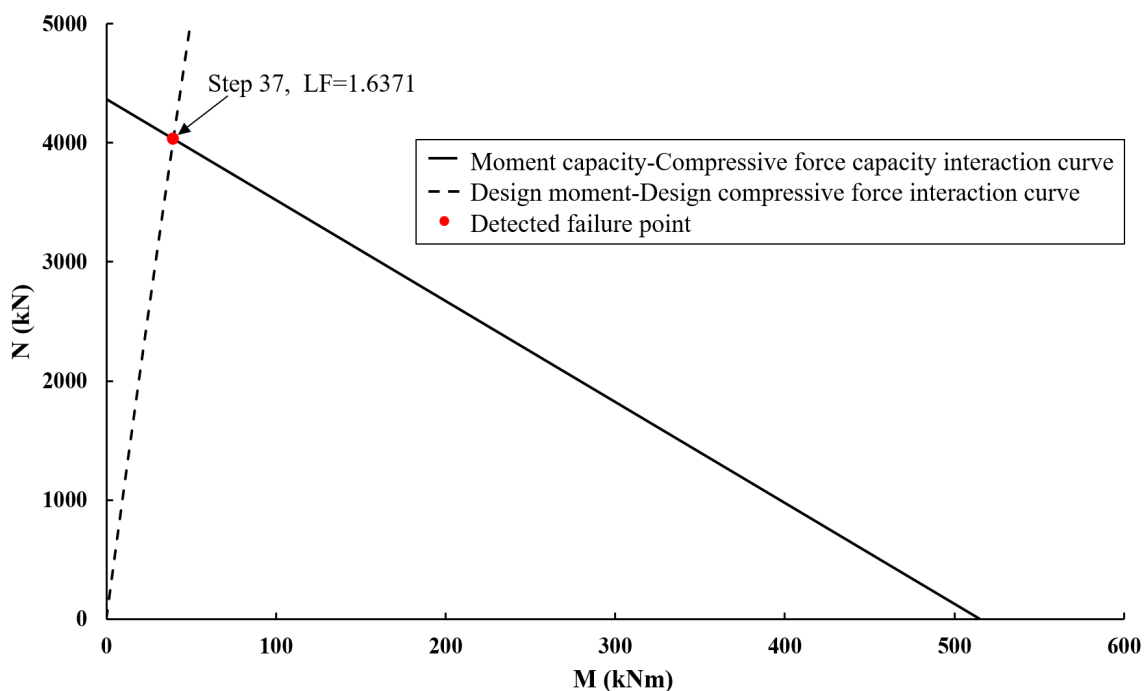


Figure 27: GNIA with linear elastic cross-section check

In the above Fig 27, the two M-N interaction curves intersect at step 37 which is representing the Eq. (2.37) can no longer be satisfied, so the ultimate capacity $\alpha_{GNIA,el}$ is taken as the load factor at step 37 during the loading process.

$$\alpha_{GNIA,el} = LF (37_{th} \text{ step}) = 1.6371$$

(5) GNIA + Linear plastic C-S check

Again, the beam FE model used by GNIA with the linear plastic C-S check was modified from the previous beam FE model, and the equivalent bow imperfection is modified in accordance with plastic cross-section verification as required by prEN 1993-1-1 shown in Table 1. The cross-section check is also based on Eq. (2.37), but the bending capacity is calculated based on the corresponding plastic modulus W_{pl} . Similar M-N interaction curves has been plotted in Fig 28 to determine the ultimate capacity.

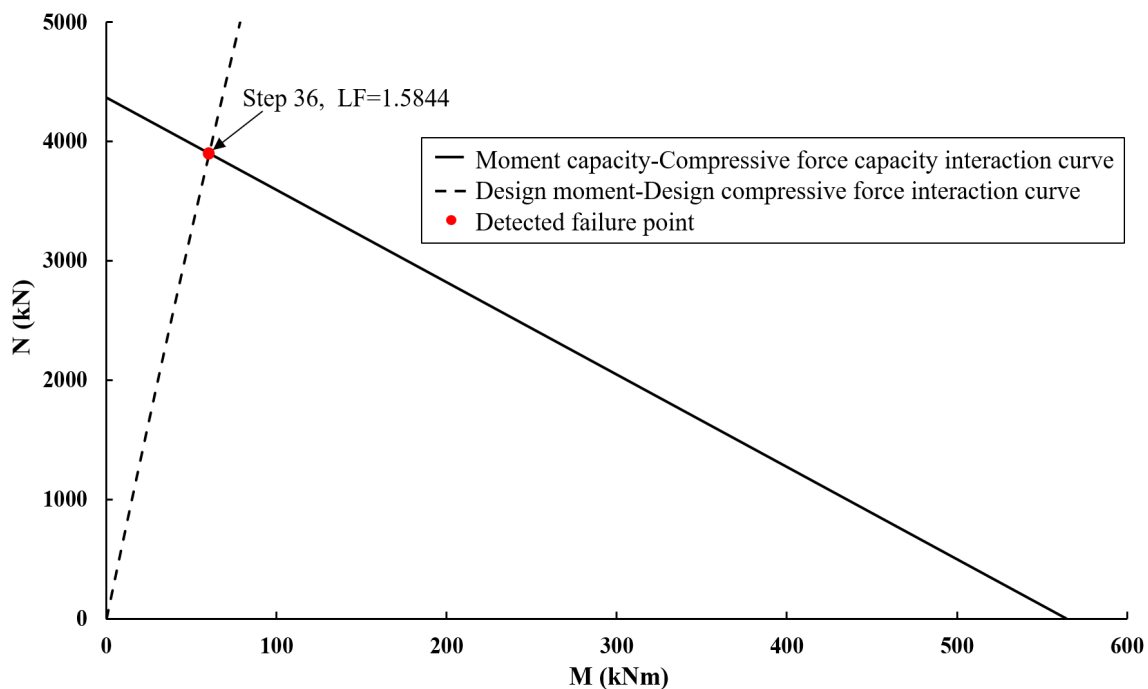


Figure 28: GNIA with linear plastic cross-section check

The GNIA with linear plastic C-S section check yields at the lowest capacity among the listed 4 different advanced analysis methods, structural failure is detected at the 36th step during the loading process, and the corresponding load factor at this step is simply taken as the ultimate capacity $\alpha_{GNIA,pl}$.

$$\alpha_{GNIA,pl} = LF (36_{th} \text{ step}) = 1.5844$$

6 Conclusion

In summary, the studied advanced analysis with CSM strain limit has been successfully extended to steel Warren truss designs, and benefits significantly by capturing the effects of strain hardening, local moment distribution, the spread of plasticity and element interaction without further design checks required. Comparing to other alternative advanced analysis methods and the conventional design approach in EN 1993-1-1, the studied CSM strain limit method completely eliminates the lengthy calculations required for cross-section classification and member capacity checks, and avoided the current limitations within truss design (effective length estimation), which will typically lead to an inaccurate ultimate capacity prediction.

The ultimate capacity predicted by the studied advanced analysis with CSM strain limit method using beam FE model has a consistent 10% to 15% capacity increment comparing to the traditional design approach, and the ultimate capacity prediction always remaining on the safe side, only 1% to 4% lower comparing to the reference shell FE model. In addition, the beam FE models used for CSM strain limits method in geometrically and materially nonlinear analysis with imperfections has successfully captured the correct failure mechanism during the analysis, which could also utilized to define the critical sections.

7 Future Work

During the relative short 2 month time, some current limitations has been identified and listed below, these limitations will be attempted to be solved in the future works shortly.

(1) Connection regions

As the current shell FE model and beam FE model cannot deal with overlapping when the two diagonal member intersects, so the truss geometry and section sizes are limited to a certain range. In the next study, the beam FE model will be attempted to account realistic connection region by recalculate the corresponding second moment of area of each divided slices in the connection region, and the shell FE model will try to include connection stiffeners to reflect realistic truss connections

(2) Parametric study & reliability analysis

In this current study, the limited results only presented some initial findings of the studied advanced analysis for truss design, and gives the author confidence for future research, but more results for different scenarios and reliability analysis are required to be carried out in order to validate that the studied advanced analysis can served well in the future as a practical design method.

(4) Complicated truss structure

Modern truss structures tend to have more complicated structural functions, the benchmark shell FE model and beam FE model need to be able to explicitly define the complicate truss geometry, connections regions and applicable for other closed sections (RHS and CHS).

References

- Chan, S. & Cho, S. (2008), 'Second-order analysis and design of angle trusses part i: Elastic analysis and design', *Engineering Structures* **30**(3), 616–625.
- Chan, S. L. & Chen, W. (2005), 'Advanced analysis as a new dimension for structural steel design', *Advanced Steel Construction* **1**(2), 87–102.
- Chen, W. F. (2008), 'Advanced analysis for structural steel building design', *Frontiers of Architecture and Civil Engineering in China* **2**(3), 189–196.
- Cho, S. & Chan, S. (2008), 'Second-order analysis and design of angle trusses, part ii: Plastic analysis and design', *Engineering Structures* **30**(3), 626–631.
- Davison, B. & Owens, G. W. (2012), *Steel designers' manual*, John Wiley & Sons.
- ECCS (1984), 8, ultimate limit state calculation of sway frames with rigid joints, in 'Tech. rep.'.
- Eurocode 3 - Design of steel structures* (2021), *prEN 1993-1-1* .
- Fieber, A. (2019), *Structural Steel Design Using Advanced Analysis With Strain Limits*, PhD thesis, Imperial College London.
- Fieber, A., Gardner, L. & Macorini, L. (2019a), 'Design of structural steel members by advanced inelastic analysis with strain limits', *Engineering Structures* **199**, 109624.
- Fieber, A., Gardner, L. & Macorini, L. (2019b), 'Formulae for determining elastic local buckling half-wavelengths of structural steel cross-sections', *Journal of Constructional Steel Research* **159**, 493–506.
- Gardner, L. (2008), 'The continuous strength method', *Proceedings of the Institution of Civil Engineers-Structures and Buildings* **161**(3), 127–133.
- Gardner, L., Fieber, A. & Macorini, L. (2019), 'Formulae for calculating elastic local buckling stresses of full structural cross-sections', in 'Structures', Vol. 17, Elsevier, pp. 2–20.
- Gardner, L., Yun, X., Fieber, A. & Macorini, L. (2019), 'Steel design by advanced analysis: material modeling and strain limits', *Engineering* **5**(2), 243–249.

- Li, Z. & Schafer, B. W. (2010), 'Buckling analysis of cold-formed steel members with general boundary conditions using cufsm conventional and constrained finite strip methods'.
- Liew, J.-Y. R. (1992), *Advanced analysis for frame design*, Purdue University.
- Quan, C., Kucukler, M. & Gardner, L. (2020), 'Design of web-tapered steel I-section members by second-order inelastic analysis with strain limits', *Engineering Structures* **224**, 111242.
- Quan, C., Kucukler, M. & Gardner, L. (2021), 'Out-of-plane stability design of steel beams by second-order inelastic analysis with strain limits', *Thin-Walled Structures* **169**, 108352.
- Walport, F., Chan, H. U., Gardner, L. & Nethercot, D. (2022), 'Design of stainless steel structural systems by GMNIA with strain limits'.
- Walport, F., Gardner, L. & Nethercot, D. (2020), 'Equivalent bow imperfections for use in design by second order inelastic analysis', *Structures* **26**, 670–685.
- Walport, F., Gardner, L. & Nethercot, D. (2021), 'Design of structural stainless steel members by second order inelastic analysis with CSM strain limits', *Thin-Walled Structures* **159**, 107267.
- Yun, X. & Gardner, L. (2017), 'Stress-strain curves for hot-rolled steels', *Journal of Constructional Steel Research* **133**, 36–46.
- Yun, X., Gardner, L. & Boissonnade, N. (2018a), 'The continuous strength method for the design of hot-rolled steel cross-sections', *Engineering Structures* **157**, 179–191.
- Yun, X., Gardner, L. & Boissonnade, N. (2018b), 'Ultimate capacity of i-sections under combined loading – part 2: Parametric studies and csm design', *Journal of Constructional Steel Research* **148**, 265–274.
- Ziemian, R. D., McGuire, W. & Deierlein, G. G. (1992), 'Inelastic limit states design. part i: Planar frame studies', *Journal of Structural Engineering* **118**(9), 2532–2549.